MICROCOPY RESOLUTION TEST CHART

BUREAU OF STANDARDS-1963-A

AFWAL-TR-87-4133

LATTICE-MATCHED HgZnTe EPITAXY DEVELOPMENT

David G. Ryding

Mercury L.P.E. Company, Inc.
Pittsburg, PA   15238

April 1988

Final Report for Period August 1986 - October 1987

Approved for Public Release; Distribution is Unlimited

MATERIALS LABORATORY
AIR FORCE WRIGHT AERONAUTICAL LABORATORIES
AIR FORCE SYSTEMS COMMAND
WRIGHT-PATTERSON AIR FORCE BASE, OHIO   45433-6533
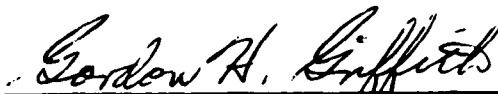
88   130

NOTICE

When Government drawings, specifications, or other data are used for any purpose other than in connection with a definitely Government-related procurement, the United States Government incurs no responsibility or any obligation whatsoever. The fact that the Government may have formulated or in any way supplied the said drawings, specifications, or other data, is not to be regarded by implication, or otherwise in any manner construed, as licensing the holder, or any other person or corporation; or as conveying any rights or permission to manufacture, use, or sell any patented invention that may in any way be related thereto.

This report has been reviewed by the Office of Public Affairs (ASD/PA) and is releasable to the National Technical Information Service (NTIS). At NTIS, it will be available to the general public, including foreign nations.

This technical report has been reviewed and is approved for publication.

ROBERT L. HICKMOTT
Project Monitor
Electronic & Optical Materials Branch

GORDON H. GRIFFITH, Chief
Electronic & Optical Materials Branch
Electromagnetic Mat'ls & Survivability Div.

FOR THE COMMANDER

SOLOMON R. METRES, Actg Chief
Electromagnetic Materials & Survivability Div
Materials Laboratory

If your address has changed, if you wish to be removed from our mailing list, or if the addressee is no longer employed by your organization please notify __AFWAL/MLPO__ , Wright-Patterson AFB, OH 45433-_6533_ to help us maintain a current mailing list.

Copies of this report should not be returned unless return is required by security considerations, contractual obligations, or notice on a specific document.

REPORT DOCUMENTATION PAGE

Form Approved
OMB No. 0704-0188

1a. REPORT SECURITY CLASSIFICATION	1b. RESTRICTIVE MARKINGS
Unclassified	

2a. SECURITY CLASSIFICATION AUTHORITY	3. DISTRIBUTION/AVAILABILITY OF REPORT
	Approved for Public Release; Distribution is Unlimited
2b. DECLASSIFICATION/DOWNGRADING SCHEDULE	

4. PERFORMING ORGANIZATION REPORT NUMBER(S)	5. MONITORING ORGANIZATION REPORT NUMBER(S)
	AFWAL-TR-87-4133

6a. NAME OF PERFORMING ORGANIZATION	6b. OFFICE SYMBOL (If applicable)	7a. NAME OF MONITORING ORGANIZATION
Mercury L.P.E. Company, Inc.		Air Force Wright Aeronautical Laboratories Materials Laboratory (AFWAL/MLPO)

6c. ADDRESS (City, State, and ZIP Code)	7b. ADDRESS (City, State, and ZIP Code)
Pittsburg, PA 15238	Wright-Patterson Air Force Base, OH 45433-6533

8a. NAME OF FUNDING/SPONSORING ORGANIZATION	8b. OFFICE SYMBOL (If applicable)	9. PROCUREMENT INSTRUMENT IDENTIFICATION NUMBER
		F33615-86-C-5085

8c. ADDRESS (City, State, and ZIP Code)	10. SOURCE OF FUNDING NUMBERS			
	PROGRAM ELEMENT NO.	PROJECT NO.	TASK NO.	WORK UNIT ACCESSION NO.
	65502F	3005	50	77

11. TITLE (Include Security Classification)

Lattice-Matched HgZnTe Epitaxy Development

12. PERSONAL AUTHOR(S)
David G. Ryding

13a. TYPE OF REPORT	13b. TIME COVERED	14. DATE OF REPORT (Year, Month, Day)	15. PAGE COUNT
Final	FROM Aug 86 TO Oct 87	1988 April	80

16. SUPPLEMENTARY NOTATION

This is a Small Business Innovation Research Program, Phase I

17.	COSATI CODES		18. SUBJECT TERMS (Continue on reverse if necessary and identify by block number)
FIELD	GROUP	SUB-GROUP	Mercury, Cadmium, Tellurium, Zinc, HgCdTe, HgZnTe, Liquid Phase Epitaxy, Tellurium Melt
20	02		
11	06		

19. ABSTRACT (Continue on reverse if necessary and identify by block number)

The technical feasibility of growing HgZnTe on CdznTe for longwave infrared applications has been demonstrated in this Phase I program. Mercury Company has developed a technique for growing reproducible large area uniform HgZnTe. The proposed research was to focus on longwave infrared (LWIR) HgZnTe, and Mercury Company routinely achieves cutoff wavelengths of 7.0 to 10.6 microns at room temperature. High quality large area Cd(0.8)Zn (0.2)Te substrates were developed by Galtech Semiconductor Materials Corporation, Utah. High resolution surface and internal IR inspection of substrates was achieved using image analysis and techniques were developed that could lead to automated inspection. In addition, SEM capabilities were developed that could lead to automated inspection of epitaxy material. (Reprint) —

20. DISTRIBUTION/AVAILABILITY OF ABSTRACT	21. ABSTRACT SECURITY CLASSIFICATION		
☒ UNCLASSIFIED/UNLIMITED ☐ SAME AS RPT. ☐ DTIC USERS	Unclassified		
22a. NAME OF RESPONSIBLE INDIVIDUAL	22b. TELEPHONE (Include Area Code)	22c. OFFICE SYMBOL	
Robert L. Hickmott	(513) 255-4474	AFWAL/MLPO	

DD Form 1473, JUN 86 — Previous editions are obsolete.

SMALL BUSINESS INNOVATION RESEARCH PROGRAM
PHASE 1 — FY 1986
PROJECT SUMMARY

Topic No. __151__   Military Department/Agency __AF__ .

Name and Address of Proposing Small Business Firm

      Mercury L.P.E. Company, Inc.
      208 Field Club Ridge
      Pittsburgh, PA 15238

Name and Title of Principal Investigator

      David G. Ryding, President

Title Proposed by Small Business Firm
      Lattice-Matched HgZnTe Epitaxy Development for Longwave
      Infrared Sensors

Technical Abstract (Limit your abstract to 200 words with no classified or proprietary information/data.)

Phase I culminated in breakthroughs in the growth of HgZnTe LPE on lattice matched CdZnTe substrates. X-ray rocking curve measurements indicate that Mercury Co.'s HgZnTe LPE has better crystal properties than that of HgZnTe reported in the literature. This is important because it has been demonstrated that HgZnTe may be superior to HgCdTe. Mercury Co. is the first to report capability of producing large area HgZnTe. Galtech Semiconductor Materials, Utah, developed and delivered large area, high quality, lattice matched for HgZnTe, Cd(.8)Zn(.2)Te substrates. X-ray rocking curve measurements varied from 19 to 32 arc seconds. Large area (30mm x 30mm) longwave HgZnTe grown on Galtech's substrates had x-ray rocking curve measurements of 50 to 80 arc seconds. The variations in the epitaxy appear to follow the substrate, indicating that as the substrate improves, the epitaxy will improve. Hall measurements were performed and the results are favorable for IR device research and development.

Anticipated Benefits/Potential Commercial Applications of the Research or Development

Mercury Co.'s HgZnTe LPE has better crystal properties than that of HgZnTe reported in the literature and is comparable to the best HgCdTe. This is important because it has been demonstrated that HgZnTe may be superior to HgCdTe. Mercury Co. is reporting the capability of producing large area HgZnTe for long wavelength infrared device research and development.

F33615-86-C-5085

TABLE OF CONTENTS

A-1

1.0 INTRODUCTION

Mercury cadmium telluride (HgCdTe) has become the material of choice for infrared (IR) detectors and focal plane arrays [1-3]. Several years ago research was undertaken on mercury zinc telluride (HgZnTe) because it was thought that HgZnTe might be superior to HgCdTe. HgZnTe has since been shown to have superior electrical and mechanical properties [4-8]. More than half a dozen papers were presented on HgZnTe at the 1986 U.S. Workshop on the Physics and Chemistry of Mercury Cadmium Telluride, October 7,8,9, 1986, Dallas, Texas. At the 1986 conference all people reporting work on HgZnTe indicated some success in growing HgZnTe and that the material has similar or superior electrical performance to HgCdTe.

Needed is large area, reproducible HgZnTe for research and development. While many organizations are capable of researching the electrical properties of HgZnTe, few are able to grow it. Indeed, HgCdTe is difficult to grow and HgZnTe may be more difficult for most to grow. The literature gives reasons ranging from lack of available lattice matched substrates to growth kinetics as possible limitations on the successful growth of HgZnTe.

Mercury L.P.E. Company, Inc. (Mercury Co.) undertook to research the liquid phase epitaxy (LPE) growth of HgZnTe on CdZnTe from a metallurgical point of view. Mercury Co. has developed a technique for growing reproducible large area uniform HgZnTe.

The proposed research was to focus on longwave infrared (LWIR) HgZnTe, and Mercury Co. routinely achieves cutoff wavelengths of 7.0 to 10.6 microns at room temperature.

High quality large area $Cd(0.8)Zn(0.2)Te$ substrates were developed by Galtech Semiconductor Materials Corporation (Galtech), Utah. The substrate material supplied for the HgZnTe was lattice matched at 10% molar zinc. $Cd(1-x)Zn(x)Te$, $x=0.20$, is 10% molar zinc and approximately lattice matches $Hg(1-x)Zn(x)Te$ with $x=0.16$ [4-8].

2.0 OBJECTIVES

The objective of this research program was to determine the feasibility of growing HgZnTe suitable for LWIR device fabrication using a liquid phase epitaxial technique. HgCdTe was to be grown for comparison. Projections of production capabilities were to be made, including throughput quantities, associated costs and projected prices per centimeter of mercury bearing LPE.

$Cd(1-x)Zn(x)Te$, $x=0.20$, was to be used as a lattice matched substrate for the longwave HgZnTe. Galtech was to evaluate and supply the substrates. Mercury Co. was also to evaluate the substrates prior to epitaxy and to determine the performance of the substrates in relation to the LPE.

3.0 TASKS

The proposed tasks of this program were to acquire and evaluate CdTe and Cd(0.8)Zn(0.2)Te substrates prior to epitaxy, polish and perform LPE on those wafers and evaluate the HgCdTe and HgZnTe.

4.0 RESULTS

Results are discussed in the text; data, photographs and plots are presented in the Appendix. Problems and their solutions are discussed, as are remaining problems and possible solutions.

4.1 CDZNTE/CDTE EVALUATION

Galtech supplied Mercury Co. with CdTe and single crystal substrates of Cd(0.8)Zn(0.2)Te. The CdZnTe received was not properly oriented and had a low count of small diameter infrared opaque artifacts, which were probably tellurium precipitates (Figures 1 to 18). Galtech resolved the orientation problem, which was an equipment technique problem due to inadequate operating documentation, and supplied Mercury Co. with 111 oriented wafers.

Using the high resolution IR techniques discussed below in the IR Microscopy section, Mercury Co. determined that Galtech still had low distribution IR visible artifacts in the large 111

oriented polished wafers. The artifacts had no effect on the successful growth of HgZnTe.

Galtech's low damage polishing is satisfactory for Mercury Co.'s LPE technique. The only pre-LPE wafer preparation employed by Mercury Co. is a simple free etch. The combination of Galtech's polished material and Mercury Co.'s LPE technique enables high volume production of Hg bearing epitaxies.

4.1.1 ETCH PIT DENSITY

Etch pit density (EPD) as determined by the Nakagawa etching technique on CdTe 111 wafers from Galtech was in the mid 10^4 range. The EPD correlates to some defects observed after application of certain LPE processes (Figure 43).

Etching of Cd(0.8)Zn(0.2)Te using the Nakagawa technique appears to give questionable results. Either the oriented 111 material from Galtech had EPD counts of only thousands per cm or the Nakagawa etch is not delineating dislocations in this high Zn material. Interestingly, the etch gives pits similar to CdTe, but on the order of thousands. There is an additional pit that does not look like a Nakagawa pit. Perfectly triangular features of the size of opaque particles observed in the IR micrographs of the same material are delineated. Besides being the same four to six micron size as the IR particles, the

distribution appears to be similar. SEM and EDS or back thinning TEM techniques may lead to a determination of these features and methods of eliminating them.

4.1.2 FTIR

Fourier Transform Infrared Spectroscopy (FTIR) was performed on the CdTe and CdZnTe. FTIR gives an indication of the electrical perfection of the materials. Theoretical transmission of 67% due to reflection from the front and back surfaces out to 15 microns indicates "clean" material. The Digilab FTIR employed had a detector with a range of 1.2 to 15 micron wavelength. Galtech's substrates routinely have 55% to 65% transmission throughout the 1.2 to 15 micron range.

4.1.3 LATTICE SPACING

Lattice spacing measurements were made using a Siemens Automatic D-500/501 Diffractometer x-ray machine with relative resolution of 0.0010 Angstrom against a given standard. A CdTe sample was kept as a standard; the lattice change from CdTe to $Cd(0.8)Zn(0.2)Te$ was 1.3%. This measurement was made at the beginning of the project when the first CdZnTe substrates arrived from Galtech. Since the equipment employs a powder technique, the orientation of the substrates did not matter. The CdTe lattice constant was 6.4510 Angstroms; the CdZnTe lattice constant was 6.3681 Angstroms (Figures 19 and 20).

4.1.4 IR MICROSCOPY/IMAGE PROCESSING

The infrared microscopic work was performed on an IBAS by Energy Technology Consultants, Inc. (ETC), Pennsylvania. The IBAS is a state of the art image analysis instrument marketed by Carl Zeiss, Inc., which can analyze images obtained directly by a television camera with a light microscope or an SEM by a television camera. An important feature of the IBAS is its versatility, which results from its being completely software driven [11]. The basis of IBAS measurements is discrimination of the objects of interest from their background; all discrimination work is in "gray levels". IR microscopy results are shown in Figures 1 through 18.

Mercury Co. requested ETC to explore IBAS IR microscopy techniques because its automated inspection capability is needed for future high volume material programs. The combination of IR and automated image analysis creates a tool that makes it possible to see the surface and internal defects in II-VI and III-V materials and perform measurements on many areas in a rapid and consistent manner independent of the operator.

To employ image processing techniques, the image is obtained with an IR television camera and stored in an image plane (computer memory). The image is then processed to give a shading correction using a low pass filter. Contrast is increased sharply by normalizing the gray level range, and edge

contrast is enhanced. These steps prepare the image for discrimination, a process that creates a binary image with two gray levels: 0 and 255. The binary image separates the objects of interest (gray level 255) from the background (gray level 0, black). The image is then refined with an erosion process; this is followed by a dilation process. The erosion process eliminates small unwanted areas in the binary image, and the dilation process returns the remaining objects to their original size. The image can be used for measuring features, including the size, areas, and shape factors of objects (Figures 21 and 22). Before the IBAS measurements are made, the objects must be identified and assigned colors. The colors are then stored in a look-up table (Figures 1-6).

The IBAS can make EPD analysis easier. The automated sampling feature can be programmed to assure that representative areas of EPDs are measured. Pit count, pit diameter and pit shape factors can then be examined (Figures 23 and 24).

An example of the surface analysis capabilities of this equipment is shown in Figures 13 and 14. The technique demonstrated can automatically categorize and/or count surface features such as scratch lines or pits. Simultaneously, the IBAS can check for opaque particles such as precipitates within the material.

Figures 15 to 18 demonstrate the IBAS's capability of performing multi-plane analysis within a material. This technique can be

used to perform three dimensional twin or grain boundary reconstruction. An example of grain boundary denudification is shown in Figure 15.

During the IR characterization of the Cd(0.8)Zn(0.2)Te, an interesting triangular or tetrahedral feature was seen. This feature was observed during analysis performed on two different ingots of CdZnTe and is shown in Figures 6, 9, 11 and 12. Because of this unusual and unreported defect, an attempt was made to determine its characteristics using TEM. The attempt was unsuccessful.

The image analysis steps described above can be done automatically after the desired program is constructed and stored on disk. The program includes a calibration factor, instructions for moving the stage and, if necessary, focusing. These features enable the instrument to scan and focus a multitude of fields and to take measurements dictated by the program without help from an operator. The data obtained is stored on disk for later analysis.

4.1.5 S.E.M.

In addition to analyzing the substrates with the IBAS, a scanning electron microscope (SEM) was used to determine bulk chemistry to within one percent. ETC has developed automated scanning electron microscopy techniques [11]. ETC has a JEOL JSM-840 SEM equipped with a LaB(6) electron gun, a light element

thin window detector and a Tracor Northern 5500 x-ray analyzer coupled with a sophisticated digital scan generator, which allows automated computer control of the microscope. The ability to quantitatively process x-ray information from both energy dispersive spectrometers (EDS) and wavelength dispersive spectrometers (WDS) allows determination of both heavy and light elements. ETC also has a Tracor Northern top of the line TN-5700 and TN-8500 analyzer. The Tn-5700 interfaces directly to the TN-5500 x-ray analyzer. This combination of instrumentation provides optimum capabilities of x-ray and image analysis because the two systems are interfaced with serial and parallel connections for fast and efficient communication. The TN-8500 is a stand alone image analysis system, which provides advanced image analysis for optical and electron microscopy imaging where no x-ray analysis is involved.

These advanced scanning and imaging SEM techniques were used on CdTe and CdZnTe. Because the SEM microprobe samples a one micron volume and the precipitates appeared to be several microns in diameter, an unsuccessful attempt was made to analyze the precipitates intersecting the surface.

The EDS was primarily used in the development of the HgZnTe. Mercury Co. is working with ETC to develop standards for measuring the Hg-Cd-Zn-Te system of epitaxies and substrates. The scanning and imaging techniques will be useful in analyzing epitaxy defects and determining if they are related to substrate defects. Plots showing relative intensities of Hg, Cd, Te and

Zn across epitaxies are given in the Appendix (Figures 25 and 26). They show a preliminary attempt at interpreting a spectrum to intermediate standards to determine atomic percent compositions. To achieve these plots, the data was put in LOTUS, renormalized and plotted.

4.1.6 T.E.M./S.E.M. and X-RAY LAUE

SEM, transmission electron microscopy (TEM) and x-ray Laue examinations of $Cd(0.8)Zn(0.2)Te$ were performed by Frank Scheltens at the University of Illinois Materials Research Laboratory (Figures 27 to 32). The TEM study showed no interesting phenomena, and a calculation of defect distribution according to the preliminary IR microscopy work predicted that more than several dozen samples would have to be prepared before an interesting area would be discovered. If advanced techniques, such as selective ion milling, are used in the future, the likelihood of discovering a precipitate in low defect material would be enhanced.

Although the IR microscope can detect IR opaque particles down to one micron size, none were detected; therefore, TEM analysis for smaller size defects was performed. TEM also showed no defects.

PRECIPITATE CALCULATIONS

The precipitate (PPT) density calculation uses the IR micrograph
and basic assumptions about TEM samples to calculate the
probability of capturing a precipitate with any given TEM
sample.

Assume:
20 = Number of PPT Visible
200 = Width of Micrograph (Microns)
30 = Diameter of Usable TEM Area (Microns)

			Number of TEM to Find One PPT		
			Thickness of TEM Sample (Microns)		
			0.5	1	2
Depth of Field (Microns)	Sample Volume (Cu. Microns)	PPT Density	TEM Sample Volume (Cu. Microns)		
			353.43	706.86	1413.72
16	6.40E+05	3.13E-05	90.54	45.27	22.64
8	3.20E+05	6.25E-05	45.27	22.64	11.32
4	1.60E+05	1.25E-04	22.64	11.32	5.66
2	8.00E+04	2.50E-04	11.32	5.66	2.83
1	4.00E+04	5.00E-04	5.66	2.83	1.41

The sample volume in the IR micrograph (100 mm x 100 mm area at
500x) is first determined for a variety of depths of field. A
PPT density is then calculated using the volumes and a PPT count
of 20 for the micrograph. The volume of a TEM sample is then
calculated based on an assumption of a 30 micron diameter usable

area, which is typical for the "no perforation technique", and three possible thicknesses for the area.

The number of TEM samples = 1/(PPT Density x TEM volume).

Based on these numbers, there is a significant likelihood of discovering a precipitate, although it may take twenty samples to do so. A typical situation is depicted in the center of the chart: the TEM sample is one micron thick and the IR micrograph has a four micron depth of field. There is, therefore, a one in ten probability of finding a precipitate.

4.1.7 GALTECH LOW DAMAGE POLISH

Mercury Co. intended to do its own polishing on the CdTe and CdZnTe substrates prior to epitaxy, but the low damage polished substrates received from Galtech required only a simple free etch. "As-received" wafers from Galtech are shown in Figure 70.

4.2 POLISHING WAFERS

Mercury Co. has an in-house low damage polishing process. Examples of Mercury Co.'s polishing are shown in Figure 70. The photograph shows counter-clockwise from the bottom left 1) "as sliced" Cd(0.8)Zn(0.2)Te, 2) similar substrates polished by Mercury Co. prior to the non-contact chemical polish, 3) Galtech wafers "as delivered", 4) Galtech wafers prepared for LPE, 5) poor LPE of HgZnTe grown while tuning the process and

6) successful longwave HgZnTe LPE. The characteristics of the epitaxy grown with Galtech or in-house polished substrates are the same.

4.3 LIQUID PHASE EPITAXY

4.3.1 HGZNTE/CDZNTE

Mercury Co. is pleased to report highly successful LPE longwave HgZnTe grown on CdZnTe (Figures 70 and 71). This material was difficult to grow. HgZnTe is less forgiving than HgCdTe (Figures 33 to 49) . This project ended with the growth of large area longwave HgZnTe with excellent surface morphology.

The high surface quality of the HgZnTe may be due to any or all of the following factors: the substrates may have better orientation or fewer defects, the LPE process may employ improved growth conditions, or HgZnTe/CdZnTe may be a better epitaxial material system. Each of these factors is discussed below.

ORIENTATION

Mercury Co. has access to equipment that allows the determination of orientation to 0.5 degree. The substrate orientation is more important for LPE of HgZnTe than it is for LPE of HgCdTe. Poor HgZnTe occurred using the non-111 oriented CdZnTe wafers; the polycrystal non-111 CdTe wafers, however, gave acceptable HgCdTe. It appears that orientation is the

critical factor. HgZnTe grown on unfavorably oriented (10 degrees off the 100) Cd(0.8)Zn(0.2)Te (Figure 49, Zn170) using the same growth conditions used for successful HgZnTe grown on properly oriented 111 substrates (Figure 47, Zn169) is very poor.

SUBSTRATE DEFECTS

Because the Nakagawa etch works only on 111 oriented CdTe and the original wafers were not 111, the Nakagawa etch could not be used to determine EPD on those wafers. The replacement wafers had 111 orientation and a Nakagawa etch was used to determine EPD. The Nakagawa etch decorates features in a manner similar to CdTe. In addition to the Nakagawa pitting, there is decoration of features that are the same size as the opaque particles in the IR micrographs shown in Figures 6, 9, 11 and 12. It is assumed that the sharpest triangular features began to etch as the particles that were slightly below the surface at the beginning of the etch became exposed. It can be inferred that the largest sharply defined triangular features are associated with the largest triangular particles seen in IR. The IR particle size distribution is shown in Figures 23 and 24.

The Nakagawa etch may not perform the same on Cd(0.8)Zn(0.2)Te as it does on CdTe. It appears that EPDs could be in the thousands rather than the tens to hundreds of thousands reported for CdTe.

- 14 -

GROWTH CONDITIONS

While growth conditions could be a factor, it is difficult to draw any conclusions at this time because Mercury Co. has not grown HgCdTe and HgZnTe under the same conditions. While HgZnTe was grown for longwave studies in this program, HgCdTe has not been attempted for longwave applications.

EPITAXIAL MATERIAL SYSTEMS

Because HgCdTe and HgZnTe are different material systems, it is not possible to grow them under the same conditions. They can be grown under similar conditions. Similar conditions would be appropriate temperature/melt chemistry, ramp rates, and x-value. A systematic study could determine if HgCdTe and HgZnTe are similar or if one is a better material than the other. Certain literature indicates that HgZnTe should be of as high or higher quality as HgCdTe [4-9].

While there was a brief flurry of interest in HgZnTe in the past several years and many reports published on its potential mechanical and electrical advantages, there has been little reported on its producibility. While a few have grown research material [4-9], no one has reported success in growing large area highly uniform material until now. The successful culmination of this Phase I effort is displayed in Figures 70 and 71.

4.3.2 HGCDTE/CDTE

HgCdTe LPE was grown on CdTe at the start of this program while Mercury Co. waited for the replacement $Cd(0.8)Zn(0.2)Te$ wafers to arrive. The time was well spent developing characterization capabilities that were later used to evaluate the HgZnTe growth process and epitaxial quality.

Due to the availability of nine square centimeter $Cd(0.8)Zn(0.2)Te$ wafers and the early success of five consecutive HgCdTe LPE growths (34 to 38), which achieved good morphological surfaces and the target room temperature cutoff wavelengths of 4.0 to 4.4 microns in the small diameter furnace, which was only capable of producing 10 x 13 mm parts, the research was transferred to a furnace capable of producing 30 x 60 mm epitaxies. The furnace scaled up according to projections but the process was not acceptably repeatable. The cutoff wavelengths and surface morphologies were varied. Cutoffs ranged from 2.7 to 4.7 microns and were usually 3.3 to 4.4 microns. The existing Mercury Co. process model suggested several upgrades to the process, which were unsuccessfully incorporated. The process model needed to be modified.

The LPE process model modifications provided the insight needed to run several experiments. Additional modifications to the model were made using the results of those experiments. The new model pointed to practical solutions to the problems. Indeed,

the first two growths of HgCdTe after the modifications at identical growth conditions that previously yielded 3.3 to 4.7 micron cutoffs produced a cutoff of 7.4 microns. Four micron wavelength material is desired for midwave infrared (MWIR) devices. Consistent cutoff wavelengths of 4.0 microns for HgCdTe are now being achieved.

IR microscopy, SEM, FTIR, x-ray diffraction and optical microscopy were developed in the first three months of the program. The LPE growth equipment was evaluated using HgCdTe because of familiarity with this material. Due to the small supply of CdZnTe wafers that was available, it was necessary to perform as many growth experiments with HgCdTe as were needed to assure proper operation of equipment before committing the limited CdZnTe supply.

HIGH QUALITY SURFACE MORPHOLOGY

To fabricate IR devices on an epitaxy, the surface must be flat. The HgCdTe grown in the B-series furnaces using Mercury Co.'s growth techniques have flat morphologies. The epitaxy is flat with slight undulations from one crystal to the next across grain boundaries in random oriented polycrystalline wafers. When oriented 111 CdTe wafers were used, the HgCdTe became flatter, even at low magnification, giving the surface a mirror effect.

CONTROL OVER HG/CD RATIO ACROSS EPITAXIAL LAYER

Mercury Co. has been intrigued by the possibility of growing HgCdTe layers with or without a change in the Hg/Cd ratio across the layer. Figures 50 and 51 show the FTIR results of etching off five microns of material. There is less than 0.05 micron change in the cutoff wavelength, from about 4.50 to 4.45. This effect is easier to see when the two plots are overlaid on a light table. Regardless of how one calculates the cutoff wavelength, the curves are the same height and are displaced less than 0.05 microns. Using the x-value relation to cutoff wavelength or bandgap, this translates to less than a 0.0005/micron change in x-value over the etched off five microns of epitaxy thickness.

Figure 25 is an EDS chemical profile across such an HgCdTe epitaxy. Mercury Co. has several variations of the LPE process, one of which gives this non-graded layer effect. If it were important to have non-graded layers Mercury Co. could probably enhance this effect, possibly to the point of mildly reversing the gradient.

SHORTWAVE (1.2 MICRON) TO LONGWAVE (10.6 MICRON) CAPABILITY

While the HgZnTe LPE process was being developed, experiments were performed on shortwave HgCdTe growths. The shortwave growths were a starting point for tuning the growth solutions for longer wavelengths. They were also done because a Hg

control problem existed. Midwave and shortwave material had inconsistent compositions. It was unclear whether the growth solution chemistry or a process problem caused the inconsistent compositions. The growth of shortwave and midwave material pointed to a process problem as the cause.

By looking at HgCdTe ranging from 1.2 to 8.0 micron room temperature cutoff wavelength, an eye was developed for the x-value. This was done by metallographic observation. This ability greatly sped up the growth iteration process. The Hg content can be estimated by examining a cleaved cross-section showing both the HgCdTe and the substrate; the higher the x-value, the shinier the HgCdTe.

Mercury Co. can grow 1.2 to 8.0 micron room temperature cutoff wavelength HgCdTe. Figure 73 is a table giving the cutoff wavelength as a function of x-value and temperature.

4.4 EPITAXY EVALUATION

Mercury Co. epitaxy characterization techniques include high resolution optical microscopy, etching, FTIR, and SEM with EDS. Hall and I-V equipment will be available in the near future. Mercury Co. is expert in metallurgical analysis of III-V and II-VI semiconductor materials. Others who are more expert and equipped to perform electrical evaluation of Hg epitaxies, particularly in relation to device performance, should examine

the longwave HgZnTe LPE generated by this project.   This would
assure fast and meaningful feedback to Mercury Co. and   others
who desire to research this material.

4.4.1   OPTICAL MICROSCOPY

EPD counts can   be made on any microscope with adequate
resolution at 200x to 500x magnification. Mercury Co. employs a
Leitz MM5 Metallograph capable of high quality pictures and
projected images at 1000x. The MM5 has a 15 inch projection
screen, which makes it easy to count the etch pits. A picture
of the image can be taken using the camera attached to the MM5
or a picture of the projection screen can be taken with a
separate camera.

The high intensity 450 watt Xenon lamp generates full spectrum
light, which allows one to use techniques such as phase
contrast, filtering, dark field, and small   aperture high
resolution imaging.   The equipment   is   capable   of 2000x
magnification when properly configured. Mercury Co. uses the
500x   setup   to   characterize   its material.   If   greater
magnification is required, a SEM, with its much larger depth of
field, is used. Results of the optical microscopy are given in
Figures 39 to 49.

4.4.2   FTIR

Fourier transform infrared spectroscopy was performed on a DigiLab FTS-20E FTIR. The instrument has one detector for 1.2 to 15 micron and another for 2 to 22 micron wavelength analysis.

Mercury Co. has fabricated HgCdTe and HgZnTe with cutoff wavelengths ranging across the 1.2 to 10.6 micron spectrum. This research was to determine the feasibility of producing HgZnTe LPE suitable for longwave infrared detector applications. Longwave applications range from 8 to 12 microns wavelength and are generally used at a detector temperature of 77 degrees Kelvin, which correlates to a room temperature cutoff wavelength of 5.5 to 7 microns.

Mercury Co. has achieved 8 to 12 micron wavelength HgZnTe LPE. The FTIR measurements were taken at room temperature. There are several equations for predicting the temperature shift due to decrease in temperature for HgCdTe; Figure 73 is a table showing the temperature shifts. The wavelength shift for HgZnTe should be similar. The wavelength shift is directly related to the bandgap shift, which is determined from the material composition and the temperature change. According to the literature, HgZn(0.16)Te has similar bandgap characteristics to HgCd(0.20)Te [4-7].

Figure 52 shows an FTIR spectra of HgZnTe with a 7.0 micron room temperature cutoff wavelength. The reported infrared

transmission spectra for longwave HgZnTe epitaxies is similar to Mercury Co.'s results [9]. The transmission edge for the lower composition Hg epitaxies is more sharply defined [9]. While the literature reports room temperature cutoff wavelengths to 6.3 microns, Mercury Co. is reporting room temperature spectra to 9 microns cutoff wavelength. The trend of longer wavelength material having less sharply defined cutoff wavelength is apparent in Figures 52 to 57.

An interesting observation of the longwave HgZnTe is the apparent cross-sectional uniformity of the epitaxy under certain growth conditions. This effect was observed while the process was being tuned for longwave material and was not verified until the final SEM EDS measurements were taken.

After the uniform composition was observed in HgZnTe, Mercury Co. analyzed several HgCdTe wafers by etching off five microns of epitaxy to determine the cutoff wavelength shift (Figures 50 and 51). The change in cutoff wavelength when five microns of epitaxy were removed was less than 0.05 microns wavelength, which corresponds to less than a 0.0005 change in x-value composition for $Hg(1-x)Cd(x)Te$ with $x=0.28$ corresponding to 4.45 microns cutoff.

4.4.3 S.E.M.

The final results for the chemical analysis are consistent, but they have not been calibrated. Standards were employed, but the

results were not absolutely correct because the Te atomic percents were always less than 50% for both the substrates and the epitaxies (Figures 25 and 26).

A correction routine was created in LOTUS 1-2-3 to give the relative ratios of the Hg-Cd-Zn-Te (Figures 56 to 61). Mercury Co. is developing standards and techniques that will give consistent and accurate absolute chemical values for the Hg-Cd-Zn-Te system.

4.5 LPE GROWTH SOLUTION FABRICATION

The LPE HgCdTe and HgZnTe grown were from a Te rich solution. The composition of the epitaxy and the growth temperatures employed to achieve such composition depend on the composition of the source solution. Ingots of HgTe, HgCdTe, CdTe and ZnTe were fabricated by mixing appropriate amounts of elemental Hg, Cd, Te and Zn together in a quartz tube. The techniques employed resulted in ingots with good uniformity of composition.

The growth solution fabrication techniques are capable of supporting production quantities. HgTe ingots larger than 400 grams are grown in one day; each of them is large enough for over 100 research growths. Larger ingots could be grown after further developmental effort.

SEM with EDS was employed to determine the ingot uniformity. Another technique used to observe growth solution uniformity was the melting temperature from run to run. Because all data was recorded, during the various stages of melting, a message was recorded along with the data acquired. Certain aspects of the melting process in uniform growth solutions were the same on each run to within seconds and to within tenths of degrees from the start of the heating process, independent of the person making the observation. This latter technique was verified during the course of the work. While a growth solution was being "tuned" for proper composition, some of the characteristic melting features changed as the solution composition was modified. For example, Cd was adjusted in the growth solution in several ways. CdTe(50/50) or Cd(10)Te(90) atomic percent was added to the solutions according to automated computer growth solution calculations. Changing the Cd ratio in this manner caused the CdTe pieces to melt at different rates and to completely dissolve at different times and temperatures during the heating process. Solution compositions were reproduced using the same ratios of ingots as were used earlier. New ingots were fabricated and the same melting features were observed as with the initial solution.

There are several advantages of using pre-reacted "calibrated" growth solutions, including ease of LPE melt weighing (weighing a solid rather than a liquid), lower cost and safety (low pressure processing and no liquid mercury). The most important

feature of pre-reacted melts is their simplicity. This technique is an integral part of the overall process and it enhances the low cost emphasis of Mercury Co.'s LPE process. Because the growth solutions are low pressure and non-explosive, Mercury Co.'s epitaxy equipment has a long life, simple design and low cost. The benefits far outweigh the extra step of fabricating the growth solution ingot.

4.6 MODELING

Mercury Co. relies heavily on modeling and is adept at computer modeling of semiconductor growth systems and thermal mapping within the material during growth. Mercury Co. has modeled its furnaces and LPE process [10].

4.6.1 MODEL OF LPE PROCESS

Mercury Co. had an adequate LPE process computer model before embarking on this project. During this project, it became evident that the model needed more detail. The LPE scale up factor from the 10 x 13 mm wafer size to 30 x 30 mm size was not detailed enough for the LPE process model, although the furnace model was accurate for thermal management. Because the LPE model is now sufficiently detailed and has been tested, Mercury

Co. can confidently project larger size furnaces and LPE processes for HgCdTe and HgZnTe.

4.6.2 MODEL OF FURNACE

Mercury Co. has expertise in the design and construction of specialty furnaces for III-V and II-VI semiconductor crystal growth. Several computer models have been written by Mercury Co. to aid in furnace design. Models help in the conception stage, guiding one to designs within practical engineering limits. Cost analyses (materials and labor) are also performed. Results from recently completed furnace research and development relevant to growing LPE are discussed in Figures 62 to 69.

LPE growers agree that temperature control and stability are extremely important [1]. Mercury Co. has focused on thermal management during LPE processing. In addition to precision temperature control and thermal profile shaping, Mercury Co. has developed the capability to measure, record and interpret temperature resolutions of 0.01 C [10]. The furnaces are tuned using at least ten thermocouples. The LPE growths are monitored with five thermocouples.

4.7 FURNACES

Five different furnaces were used in this study for LPE and growth solution fabrication. The first furnace was a "standard" three zone furnace, #C1, which is a symmetrical cylindrical design. Examples of #C1's temperature profile are shown in Figures 62 to 64. The second furnace was a symmetrical cylindrical "shaped zone" furnace, #C2, and was used to fabricate growth solutions and to study a VPE technique. The results from the VPE study led to the design and construction of a third furnace, #C3, a cylindrical three zone furnace, which should allow a faster VPE process and fabrication of larger growth solution ingots. VPE research with furnace #C2 has begun and the initial growths show promise. Furnace #C3 is operational and grows VPE faster than #C2. The fourth furnace used was #B1, which is a non-symmetrical four zone furnace. The fifth furnace used was the production model, #B2, which is a four zone non-symmetrical furnace capable of three inch diameter epitaxy.

4.7.1 STANDARD FURNACE

A standard three inch core furnace (#C1) with a two centimeter diameter quartz LPE containment tube was used at the start of this program; results were varied and usually poor. The gradient in the furnace was initially a problem, but that was solved by adding a special front and end zone to the existing furnace (Figure 64). The most serious problem was the inability to watch the melt and wafer during the heat-up, melt-on, and

melt-off steps. The ability to directly view the process during the development stage greatly speeds up the solving of problems. For example, the wafer must be covered with the melt during the LPE process. In the beginning, several runs were made where the melt did not move onto the wafer or where it moved off of the wafer during the growth. These problems were remedied with a steeper tilt angle at the start of growth and a redesigned LPE boat. Now that the LPE process is understood and capable of automation, a "blind" standard furnace could be used in the LPE process if desired.

The second furnace, #C2, was used for growth solution fabrication and VPE studies. Mercury Co.'s VPE technique is a vertically oriented research and development process designed for 10x10mm size parts. The VPE process was slow compared to LPE. To speed the VPE process, several additional thermodynamic considerations were designed into #C3, which was constructed and temperature profiled successfully [10]. VPE of HgZnTe 20 microns thick has been grown in furnace #C3 in less than four hours. Research and development are needed to determine growth parameters to control the chemical composition of the epitaxy.

4.7.2 FURNACE #B1: 10 X 13 mm PARTS

Furnace #B1 was designed to incorporate several interesting features. It is a four zone furnace with a three inch long temperature "flat zone". It is controlled by a single

inexpensive one zone controller and has temperature ramping capability of 0.01 degrees C per minute to degrees C per minute and steady state temperature stability better than + or - 0.02 degrees fluctuation. It achieved all of the above due to systematic modeling, flexible construction, testing, remodeling and reconstructing. This iterative process is carried out three to five times while Mercury Co. is developing a furnace [10].

At the time of proposal submission, only one centimeter Cd(0.8)Zn(0.2)Te was available. Mercury Co. designed furnace #B1 with this consideration in mind. Furnace #B1 is designed to yield 10 x 13 mm parts. After Galtech entered the CdTe commercial market, for the first time, large area Cd(0.8)Zn(0.2)Te became available. Mercury Co. made use of Galtech's large area wafers for HgZnTe epitaxy.

With the successful growth of several HgCdTe epitaxies in a row, numbers 34-38, Mercury Co. decided to continue the HgZnTe project in the production furnace (#B2).

4.7.3 FURNACE #B2: 30 X 60 mm PARTS

Furnace #B2 is a four zone furnace designed to process a three inch diameter quartz tube [10]. The flat temperature zone is 10 to 12 inches long (Figure 69). This multi-zone furnace runs on a simple single zone controller. It was designed this way because of its low cost, ease of operation and improved control (no thermal crosstalk between zones affecting control). Most

important, the design allows easy reproduction of the furnaces enabling high volume epitaxy production.

Advantages of a large flat zone are apparent to those familiar with LPE. Most state that it is necessary to maintain temperatures to within 0.1 C over the growth area [1]. Temperatures in furnace #B2 are to within 1.0 C over ten inches without tuning the end zones. This flat property could be used in slider LPE arrangements where the boats need to be longer in order to accomodate the multiple well capability.

5.0 TECHNICAL FEASIBILITY

The technical feasibility of growing HgZnTe on CdZnTe for longwave infrared applications has been demonstrated in this Phase I program. Galtech's CdTe and Cd(0.8)Zn(0.2)Te were proven to be viable substrates for HgCdTe and HgZnTe, respectively. Mercury Co. and ETC achieved high resolution surface and internal IR inspection of substrates and developed techniques that could lead to automated inspection. In addition, SEM capabilities were developed that could lead to automated inspection of epitaxy material.

5.1 GALTECH INC. CDTE/CDZNTE

Mercury Co. was impressed with the quality of Galtech's substrate materials. The high quality CdTe and Cd(0.8)Zn(0.2)Te

performed well when HgCdTe and HgZnTe epitaxy were grown on them.

5.2 HGCDTE

HgCdTe LPE was grown using advanced Mercury Co. furnaces. The cutoff wavelengths were intentionally grown from 1.2 to 7.3 microns with excellent surface morphology and layer composition uniformity. The uniformity of the chemical composition across the layer is demonstrated in EDS Figures 60 and 61. The change in cutoff wavelength when five microns of epitaxy were removed was less than 0.05 micron, which corresponds to less than a 0.0025 change in x-value over five microns of epitaxy. This is less than a 0.0005 x-value change per micron, for $Hg(1-x)Cd(x)Te$ with $x≈0.28$ corresponding to 4.45 micron cutoff (Figures 50 and 51).

5.3 HGZNTE

Great success was achieved in growing high quality, large area, longwave HgZnTe. The surface morphologies are excellent. (Figures 39 through 49). The material was grown and chemically processed to exacting dimensions (12 microns thick), as demonstrated in Figures 54 and 57, which show FTIR results from epitaxies Zn169 and Zn173. Both epitaxies were grown under the same conditions and were 23 microns thick. The wafers were then broken in half and 11 microns were etched off; the final

- 31 -

thickness of each was 12 microns. This thickness will allow comparison with 12 micron thick material grown by others.

The FTIRs of Zn 169 and 173 are identical. This demonstrates that longwave material can be successfully reproduced. These parts have cutoff wavelengths of 7.3 microns at room temperature, which translates to 13.2 microns at 77K (Figure 73).

6.0 POTENTIAL POST APPLICATIONS

Mercury Co. is a commercial source of HgCdTe and HgZnTe epitaxies for research and development and is capable of participating in production programs. Mercury Co. presents results of its low cost, high volume, production LPE study in Figure 72.

Mercury Co.'s epitaxies could also be grown on the alternate substrates being developed. This would result in lower costs per centimeter than discussed in Figure 72. The Mercury Co. epitaxy process is designed to scale up to three inch or larger diameter wafers. Because the process and equipment are simple and cost effective, production can be scaled up quickly and economically.

Most exciting is that more organizations could participate in IR device research and development without having to bear the cost and risk associated with a complex materials technology

program. With the exception of Mercury Co., all growers of HgCdTe also make devices. Mercury Co. is not reluctant to supply epitaxy material in large volumes for device fabrication.

7.0 RELATION TO FUTURE RESEARCH

Precision furnaces grow better epitaxy [1]. Mercury Co. has such furnaces and the technology to increase the size and performance of furnaces for epitaxy processing [10]. The Mercury Co. furnace designs can be upgraded to accomodate slider boats capable of processing three inch diameter wafers. The temperature profile can be controlled to better than 0.02 C over distances greater than ten inches and, with research and development, this performance could probably be extended to any length desired. Slider boat epitaxy techniques permit heterolayer materials to be processed. The Mercury Co. furnace design would be useful in the research and development of LPE heteroepitaxies.

Organizations can now acquire large area longwave HgZnTe to research its electrical and mechanical properties. Electrical and mechanical measurements are time consuming, expensive, and frequently subject to interpretation and/or technique. It is suggested that many work on these analyses of HgZnTe with material supplied by Mercury Co. In addition, the ability to dope such material is needed. Mercury Co. research and development techniques are well suited to this LPE task.

- 33 -

The Mercury Co. LPE process is flexible. There are many variations of the process that produce the same cutoff wavelength material. It has not been determined at this time which process produces better material. Because the industry accepts device results as the most meaningful, devices could be fabricated and tested on the large area material. Fabricating devices allows a material uniformity analysis and, simultaneously, a producibility assessment. Results of these analyses would allow a determination to be made of HgZnTe as a future IR material.

8.0 REFERENCES

[1] R.E. Starr, P.E. Herning, M.H. Kalisher, and R.J. Carralejo, Santa Barbara Research Center, Final Report for Period September 1978 to May 1982, AFWAL-TR-82-4141, "Growth Of HgCdTe By Liquid Phase Epitaxy For 4.6 Micron Photovoltaic Applications", AFWAL Contract No. F33615-78-C-5226.

[2] P.R. Norton, D.D. Thornton and C.L. Topper, Santa Barbara Research Center, Final Report for Period September 1978 to May 1982, AFWAL-TR-82-4142, "Photoconductive HgCdTe For 4.6 Micron", AFWAL Contract No. F33615-78-C-5226.

[3] R. Andrew Wood, Honeywell Corporate Technology Center, Final Report for Period January 1980 - August 1982, AFWAL-TR-82-4176, "Open-Tube Slider LPE Growth Of (HgCd)Te", AFWAL Contract No. F33615-77-C-5142.

[4]   A.   Sher, SRI International, A.B. Chen, Auburn   University,
W.E.   Spicer,   Stanford   University,   "Dislocation Energies And
Hardness Of Semiconductors", Appl.   Phys. Lett. 46(1), 1 January
1985, pg. 54.

[5]   M.A.   Berding,   S.   Krishnamurthy,   and   A.   Sher,   SRI
International, A.B. Chen, Auburn   University,   "Electronic   Band
And Transport Properties Of HgCdTe And HgZnTe", Proceedings 1986
U.S. Workshop on the Physics   and   Chemistry   of Mercury Cadmium
Telluride.

[6] D.   Chandra   and H.F. Schaake, Texas Instruments, "Growth Of
HgZnTe By LPE", Proceedings 1986   U.S.   Workshop   on the Physics
and Chemistry of Mercury Cadmium Telluride.

[7] S. Sen, W.H.   Konkel,   R.C.   Cole, T. Tung, J.B. James, E.J.
Smith, V.H. Harper, and B.F.   Zuck,   SBRC,   "Crystal   Growth And
Properties Of Bulk HgZnTe: A New Alternative", Proceedings 1986
U.S. Workshop on the Physics   and   Chemistry   of Mercury Cadmium
Telluride.

[8] S.   Sen,   W.H.   Konkel, R.C. Cole, T. Tung, J.B. James, E.J.
Smith,   V.H.   Harper,   and   B.F. Zuck, SBRC, "Epitaxial Growth,
Characterization, And Phase Diagram Of HgZnTe", Proceedings 1986
U.S. Workshop on the Physics   and   Chemistry   of Mercury Cadmium
Telluride.

[9] Ariel Sher, D. Eger, and A. Zemel, Soreq Nuclear Research Center, Israel, "Mercury Zinc Telluride, A New Narrow-Gap Semiconductor", Appl. Phys. Lett. 46 (1), 1 January 1985, pg. 59-61.

[10] D. Ryding, Mercury L.P.E. Company, Inc., "Precision Furnaces For III-V And II-VI Semiconductor Crystal Growth", Ben Franklin Partnership Challenge Grant Program For Technological Innovation, Agreement No. 410168-45198-356-001.

[11] E.N. Silverman, Energy Technology Consultants, "Development Of Automated Microscopy Methods To Characterize Process Induced Damage In II-VI/III-V Compounds".

9.0 APPENDIX

SUMMARY OF FIGURES PRESENTED IN THIS REPORT

Figure 1. The IBAS is a state of the art image analysis instrument marketed by Carl Zeiss, Inc., which can analyze images obtained with a television camera, a light microscope or SEM with a television camera. The camera shown permits IR viewing at 1.2 micron wavelength.

Figure 2. Figure 2 is a Polaroid picture of the IBAS viewing screen showing an opaque particle or precipitate distribution in a wafer of Cd(0.8)Zn(0.2)Te. A printout of the particle count and particle diameter distribution is shown in Figure 23. The image has been processed to enhance the particles. The irregular enclosed areas are drawn by "mouse" control and are used to give a diameter and area distribution of the clear areas. The clear areas are thought to be the cellular structure. It is possible to recreate only the cells in three dimensions with more sophisticated software.

Figure 2 had 243 particles, which was too many to count by hand; the IBAS was programmed to automatically eliminate the out of focus features before the count was made. The few remaining questionable features were manually eliminated before the count was made.

Figure 3. Figure 3 shows the first step in discriminating the enclosed areas, contrast enhancement.

Figure 4. After contrast enhancement, the enclosed areas give a gray level of 255 (or black). Because nothing else is completely black, the enclosed areas will be the only remaining features after the erosion process eliminates unwanted features.

Figure 5. Only the enclosed areas remain. Diameter and area distributions for Figure 5 are given in Figures 21 and 22.

Figure 6. Figure 6 was taken at 400x and shows triangular or tetrahedral particles. The particle diameter distribution is given in Figure 23.

Figure 7. The next series of IBAS photographs were taken with the 35 mm attached camera. Figure 7 shows a high distribution of particles or precipitates at 25x. The count and diameter distribution are not given for this picture, but they are similar to those given above for Figure 2. The particles are three to ten microns in diameter. The cellular structure can still be observed.

Figure 8. Figure 8 was taken at 100x and shows the same area as Figure 7. As a result of the automatic elimination of unwanted

features, the uniform particle size and cellular structure is easily observed.

Figure 9. Figure 9 was taken at 400x and permits observation of the triangular or tetrahedral features, which are four to six microns in diameter. The image was processed differently than those described above in order to sharpen the features of interest.

Figure 10. Figure 10 was taken at 800x and is a 2x image magnification of a 400x picture. The 400x image is stored and one quadrant is made to fill the screen. The cluster was examined closely because this type of cluster occurs often and it appears that the particles sit on corners of a three dimensional tetrahedral. This appearance is more obvious when the image is looked at in real time while moving the focus in and out slightly. Another technique used to make this observation was the storing of several slightly different focused images in the IBAS image storage planes and the quick retrieval of them in continuous succession.

Figure 11. Figure 11 is another photograph taken at 400x and shows the five micron triangular features.

Figure 12. Figure 12 shows the triangular cluster pictured in Figure 11 at 800x. Only the feature in the center of the cluster is in sharp focus and it retains its sharp perimeter. The other particles have degraded because they are slightly out of focus.

Figure 13. Figure 13 portrays an attempt to determine surface scratches automatically using IBAS routines. At the beginning of the HgZnTe LPE growth research, scrap wafers were used to iterate the LPE process. The polish was poor on many of the parts used at that time and those parts were used in the scratch determination experiment. The scratches were removed from the image, allowing observation of the precipitates in crystallographic directions. (Figure 14).

Figure 14. Figure 14 is Figure 13 with the surface features or scratches removed by image processing. It was possible to remove the scratches because the gray level of scratches, which are all on the surface, is different from that of the precipitates lying some small distance below the surface. By focusing slightly below the surface, storing the image and processing it to enhance the gray levels of only the particles of interest, the scratches were removed. The precipitates decorating crystallographic orientations can be more easily observed by processing several images at slightly different depths, storing them and retrieving them in rapid succession. This technique permits one to look into the material along a linear feature, which is a crystallographic feature, e.g., twin, etc. As some particles come into focus, others go out of focus. Because these particles are not on the surface, the remaining lines are also not on the surface.

The surface features/scratches can now be readily analyzed. The IBAS can subtract the image shown in Figure 14 from that shown in Figure 13 thereby creating a new image, which can then be enhanced to analyze the surface features. This technique could be developed for quality control at various steps in a production environment and would be helpful in the development of production polishing techniques.

Figure 15. Figure 15 is an example of a denuded zone along a grain boundary.

Figure 16. Figure 16 shows many linear precipitate decorated features (slip lines?) ending at an invisible grain boundary. The rectangle is placed so analysis is limited to the features within its boundaries. This enables selective analysis to be performed. An enclosure can be generated by placing points at opposite diagonals and letting the IBAS draw the rectangle or by drawing the enclosure by hand with a "mouse" or "light pen".

Figure 17. Figure 17 shows an unprocessed image of the area shown in the square in Figure 16. The particles lie along a line, which is slightly visible in places.

Figure 18. Figure 18 is a processed image of Figure 17. Because the crystallographic plane on which all of the features are distributed angles into the wafer, only a small region can be focused on at one time. The focal plane of the microscope intersects the plane containing these features. The depth of field at 400x is only one micron. To count particles per unit volume, only the particles and volume that are in focus may be counted and calculated. To obtain particle dimensions such as diameter and area, again, only particles in focus may be used. Particles that are out of focus tend to look larger.

Figure 19. Figure 19 shows the x-ray powder diffraction analysis for CdTe. The highest intensity corresponds to the 111, which is 3.7245 two theta - d spacing. The d spacing multiplied by the square root of three (1.73205) gives the lattice spacing:

$$3.7245 \times 1.73205 = 6.4510 \text{ Angstroms.}$$

Figure 20. Figure 20 is the analysis of Cd(0.8)Zn(0.2)Te lattice spacing. The 111 spacing corresponds to 3.6766 x 1.73205 = 6.3681 Angstroms, which is a 0.0829 Angstrom difference. This is a 1.3% shrinkage from that of CdTe.

Figure 21. Figure 21 is an IBAS histogram of DMAX, which is the distribution of measured objects diameters. The y-axis is the number of objects of a given size and the x-axis is the diameter of the objects in microns. Figure 21 is an analysis of the cellular structure of the Cd(0.8)Zn(0.2)Te shown in Figures 2 through 5. Cellular diameters are centered around 100 microns.

Figure 22. Figure 22 is an IBAS histogram of the area of the objects in Figures 2 through 5 in square microns. The cross-section area of the cells is generally 10,000 square microns.

Figure 23. Figure 23 is a DMAX histogram of the diameters of the particles shown in Figure 2. There are 243 particles analyzed in Figure 2. The diameters range from 5 to 13 microns and the distribution is centered around 8 microns. The IBAS prints information requested by the user at the right of the plot. The number of particles counted is given at the top right. The minimum, maximum and mean diameters are printed, along with the standard deviation. The maximum diameter is 17.5 microns, but there are only one or two counts in these bins of the histogram. The user can ask the IBAS to indicate those particles and then he can decide if those particles should be used in the analysis. If two particles are overlapping during the analysis, they give the appearance of one large particle because the image of the combined particles is continuous. The IBAS can be programmed to examine the larger particles for proper shape and in-plane focus before counting them in the analysis.

Figure 24. Figure 24 is a histogram showing the distribution of the cross-sectional area of the particles shown in Figure 2.

Figure 25. Figure 25 is a plot of the relative x-ray intensities using energy dispersive spectroscopy (EDS) of a HgZnTe epitaxy (Zn165). Zn165 was eight microns thick. The relative intensity factor scale indicates that Te is 1.0 across the epitaxy and the substrate, which it should be because Te is fifty atomic percent in the substrate and epitaxy. The Hg signal is high near the surface, which may be a surface effect of the epitaxy, and the zinc signal is low near the surface. At the epitaxy to substrate interface the Hg signal drops to zero, the zinc signal drops slightly and the cadmium signal rises from zero to its substrate value. The substrate should be $Cd(0.8)Zn(0.2)Te$.

This plot illustrates a Hg composition gradient through the epitaxy layer. There is an error in the zinc trend because it should increase in the substrate. The EDS was not calibrated for Hg-Zn-Cd-Te analysis; however, the analysis is still useful to examine the Hg trend in the epitaxy. The SEM and EDS were most useful in determining the composition of the surface defects as shown in Figures 33 to 38. An understanding of these features helped to eliminate them, thereby leading to the successful growth of longwave HgZnTe.

Figure 26. Figure 26 is a relative intensity EDS plot for HgCdTe on a CdTe substrate. This plot illustrates the flat composition profile that can be achieved with Mercury Co.'s LPE techniques.

Figure 27. Figures 27 through 32 were created by Frank Scheltens at the University of Illinois Materials Research Laboratory.

Figure 27 is a SEM of a chemically prepared surface of a CdZnTe substrate and shows several features. These features are the same size as the particles observed in the IR micrographs described above in Figures 6 and 9-12. An attempt was made to chemically analyze the features with EDS, but they were indistinguishable from the bulk material. Either the features have the same or similar chemical structure as the bulk material or they are thin and consist of the same elements found in the bulk material but in different ratios. A study could be performed to determine which is the case. Indeed, ETC could use automated SEM mapping techniques to look for such features, chemically analyze them and run statistics in an attempt to characterize these features. This would be useful if one needed to know the composition of the particles to adjust the process to remove them, if possible.

Figure 28. Figure 28 shows an electron channeling pattern (ECP). The sample was tilted approximately ten degrees to bring the high symmetry pole into coincidence with the beam direction. The symmetry of the pole is four-fold, which is consistent with the 100 direction. In addition to identifying crystal orientations, the ECP technique can be used to give an indication of relative crystal perfection from sample to sample. The indication of crystal perfection is given by the number and clarity of the lines in the pattern. Dislocation densities corresponding to deformation levels on the order of 1% to 2% will blur the fine lines of the channeling pattern indicating a loss of crystal perfection. This technique may be useful for future analysis of epitaxial layers and substrates with levels of dislocation density on this order.

Figure 29. Figure 29 shows a TEM photograph of $Cd(0.8)Zn(0.2)Te$. The sample was prepared for TEM by chemically thinning with a 1% Bromine 99% Methanol solution. The 3mm disks were mechanically dimpled prior to chemical polishing to insure center perforation. An attempt was made to perforate the sample inside a high density field of the precipitates shown in the above IR micrographs. The majority of the samples were taken from different areas of the same wafer.

The bright-field micrograph in Figure 29 is representative of the three samples examined. No precipitates were found in the three samples and only one contained any dislocations. The molted looking decoration in the background is surface structure, which is not an unusual phenomenon with chemically polished TEM samples. It is possible that this surface structure could be removed without damage by low Kev cleaning in the Precision Ion Miller (PIM). The PIM could also be used to selectively thin an area to examine an interesting feature such as a precipitate.

Figure 30. Figure 30 shows a selected area diffraction (SAD) pattern representative of the examined samples. The highly visible Kikuchi lines indicate a thick sample, which is found

when a "no perforation" preparation technique is employed. This preparation technique was used to achieve the largest sampling volume to try to locate one of the sparse precipitates.

Figure 31. Figures 31 and 32 show back-reflected Laue x-ray diffraction patterns for two different orientations of the same wafer. Figure 31 was taken with the crystal at zero rotation (i.e., facing directly at the film), and it shows the amount of misorientation from the adjacent high symmetry pole. The amount of misorientation can be calculated as follows:

$$ON/OC = TAN(2 \times ALPHA)$$

Where: ON = crystal to film distance
           OC = film center to spot distance
        ALPHA = amount of angular displacement

So: 11mm/30mm = TAN(2 x ALPHA)
       ALPHA = 10.07 degrees

The Laue photographs in Figures 31 and 32 have been magnified 1.5 times.

Figure 32. Figure 32 was taken with the crystal rotated 10 degrees toward the high symmetry pole to remove the uneven distortion and make it easier to identify the symmetry. The symmetry can be recognized as four-fold, which is characteristic of the 100 direction. The 111 would show six-fold symmetry.

Figure 33. Figure 33 shows a SEM micrograph of a 30 micron thick HgCdTe epitaxy. EDS measurements were taken across similar HgCdTe epitaxies and the composition profiles were plotted (Figures 60 and 61).

Figure 34. Figure 34 illustrates the calibration markers showing 10 micron (0.01mm) spacing between each division. Figure 34 is a 500x photograph taken on a Leitz MM5 metallograph. This particular calibration photograph can be used to measure features in this report.

Figure 35. Figure 35 is a 500x micrograph of one of the first successful HgZnTe longwave epitaxies (Zn166). The entire Zn166 wafer is displayed several times in this report. It had many problems, which were analyzed in detail, and some will be discussed in the following figures.

Figure 36. Figure 36 is a SEM micrograph showing an EDS technique employed to determine the chemical composition across an epitaxy and substrate. This particular figure demonstrates a one micron stepping and the results are plotted in Figure 25. At the time this micrograph was taken, the SEMs employed for these measurements did not have the software or standards required to give an absolute chemical evaluation; therefore, relative intensity distributions were plotted. By the end of this

program, the software and standards had been developed and the absolute chemistry was determined (Figures 58-61).

Figure 37. Figure 37 depicts the defect features observed on the surface of epitaxy Zn166. Because the cleaved cross-section was analyzed and shown to be microscopically uniform to within the resolution limits of the EDS, it can be assumed that the larger features shown in Figure 37 were deposited on the surface at the end of the growth. Not shown are large features (millimeters) called "melt spots". Melt spots can happen when irregular surface features are large enough to disturb the melt's surface tension during a pour-off or a wipe-off.

A feature of particular interest in Figure 37 is in the center of the picture; it consists of Hg,Te and Zn. The mechanism causing this feature has not been completely determined, but growth techniques to eliminate it have been developed. The Hg to Te ratio is approximately that of the bulk epitaxy and the Zn ratio is about one third that of the bulk epitaxy. Therefore, it is not a melt spot.

Figure 38. Figure 38 shows two other features of interest in Zn166. They are seen in Figure 37 at a location of seven to eight o'clock compared to the centered large feature. The flat circular feature is a HgZnTe composition with approximately the same proportions of Hg and Te as the bulk epitaxy but with only one fourth the Zn.

The columnar feature in the upper left has varying compositions from its base to its tip. Immediately above the base, the composition is HgZnTe with the same Hg to Te ratios as are found in the bulk epitaxy and with a Zn ratio slightly more than half that of the bulk epitaxy. The center of this feature has a slightly higher Te count than the bulk epitaxy and the Zn is one third that of the bulk epitaxy. The top of this feature is shown in Figure 39 and it consists only of Hg and Te.

Reasons for these features have not been determined, but techniques to eliminate them have been developed. While these features have been eliminated using sophisticated iterative techniques, an understanding of the mechanism responsible (e.g., threading dislocations?) would allow the improvement of epitaxy performance and the quick development of a new epitaxial material system.

Figure 39. Figure 39 is a close-up of the top of the feature shown in the upper left corner of Figure 38. It is a HgTe composition, favoring Te. There is no Zn detectable using EDS.

Figure 40. Figure 40 shows two of the last six successful HgZnTe growths. Wafer Zn168 reflects the Mercury Co. business card. To its upper right is wafer Zn166. The numbering sequence is by the furnace run and is independent of the material being grown. A prefix is added such as Zn or Cd if it is HgZnTe or HgCdTe.

Cd167 was between Zn166 and Zn168. Six successive successful HgZnTe growths were 166, 168, 169, 171, 172 and 173. The results from defect analysis of 166, which is still a success because of longwave cutoff and good surface morphology, except for the defects presented here, and the five remaining successful growths are presented below. All of these wafers are 30 x 30mm.

Figure 40 also shows IR photographs at the upper right of the substrates employed in the HgZnTe successes. The FTIR traces of the HgZnTe epitaxies are on the table. A SEM micrograph of Zn166 is at the front of the picture.

Figure 41. Figure 41 is a 50x micrograph showing an edge area of Zn168. Each picture frame is 5mm across. Figure 41 demonstrates the good surface morphology of the longwave HgZnTe epitaxies. The edge of the epitaxy shows terracing, while several millimeters from the edge the epitaxy is flat. Terracing at the edges could result for many reasons. Orientation effect due to edge rounding of the substrate from the free etch is the most likely.

Zn 168 was 18 microns thick. Figure 41 is representative of the edges and the center area of the entire 30 x 30 mm epitaxy.

Figure 42. Figure 42 is a 100x picture of Zn168 showing the flat surface morphology and a defect. There were only a few such defects on the entire wafer. Their cause has not been determined, but similar defects in HgCdTe have been reported [3].

Figure 43. Figure 43 shows a portion of the large flat area where a mild terracing effect was observed. It is a 200x micrograph with the highest contrast attempted. The growth platelets tend to be pinned at the tiny one micron size pits. This same phenomenon has been observed in Mercury Co.'s HgCdTe, which is grown with a similar technique and the same equipment. If such pit features were not present, the surface would be completely flat, as is the case over the majority of this wafer's surface. While the pits can be observed over the whole wafer, the terracing is not obvious. Some does exist, and if in/out focus techniques are used at pit locations, mild terracing will be seen.

The flatness of the epitaxy may be the result of the substrate orientation, the CdZnTe lattice matched substrate or the Mercury Co. process. Large individual growth platelets (occasionally millimeters in size) can be observed in places. It is unknown why this phenomenon was seen on some of the random oriented polycrystal CdTe used during the HgCdTe equipment shake-down growths.

The pits form a pattern that suggests the "cellular" pattern sometimes observed in CdTe substrates when an EPD count by Nakagawa technique is performed. Mercury Co. also observed this

pattern when it performed HgCdTe LPE on CdTe substrates. The question remains whether these mild epitaxial pits are dislocation associated. If that is the case, then the dislocations can be counted directly from the epitaxy. Whether the cause of the pitting is growth effects or thermal etching after growth remains to be determined. Similar pits have been observed in epitaxies grown by others, but have not been so clearly delineated as by this growth technique. Perhaps the pits have alway been present but have been masked by the growth techniques. Device performance will determine which growth techniques produce better epitaxy.

Figure 44. Figure 44 is a 25x micrograph of a crystallographic surface effect. Large area "defect" features are usually observed at low power using phase contrast microscopy rather than at high power because there is more area in which to observe phase related effects. The triangular features appear to be growth platelets and are the same height as the surface.

Figure 45. Figure 45 shows a triangular intersection between platelets at 100x and illustrates plate pinning due to the one micron size pits.

Figure 46. Figures 46 to 48 show the same twinned area on three epitaxies (162, 169 and 168) after HgZnTe epitaxy was grown by different techniques. The LPE processing techniques were varied in a controlled manner and, as a result, the wavelength was successfully increased.

Figure 46 is a 100x picture of Zn162 at a twin boundary. The drastic change in morphology between the two 111 surfaces should be noted. It appears that the large flat growth area at the bottom of the picture is the 111 Te face. At 100x, the twinned region looks rougher than the remainder of the epitaxy. At 500x, the twinned region of Zn162 is smooth at the microscopic level (it is smoother than that of Zn168, which is shown in Figure 48). The twinned and normal regions are the same height in Zn162.

Figure 47. Figure 47 is a 100x picture of Zn169, which is the same twinned area on an adjacently cut CdZnTe substrate. The epitaxy of the twinned region is much rougher and the two areas are not the same height. The twinned area is higher by about 10% to 20%. The surface undulation accounts for the 10% to 20% variation. The surface is extremely faceted. The facets are tetrahedral in appearance. In the boundary region between the two crystals (twinned and normal), the good region appears to be slightly repressed. This could be caused by depletion of certain species in this region due to the fast growth of the twin. This orientation phenomenon is illustrated more clearly by Zn170, which is 10 degrees off the 100 and significantly different from the 111 orientation (Figure 49).

- 45 -

Figure 48. Figure 48 is a 500x micrograph of Zn168 and shows the twinned area. The twinned area is smooth at high magnification, but it has a slight undulation. This 500x picture shows more defects within the twinned area than outside it and is representative of the whole wafer. As with Zn162, the twinned and normal areas are the same height.

Figure 49. Figure 49 is a 500x cross section showing Zn170. Zn170 is over 38 microns thick and appears to be an extremely poor epitaxy from the surface. The melt covered the surface because of the high number of large facets that occurred during growth due to the orientation. The irregular features broke the surface tension of the melt and because the whole surface had a continuous spread of such features, the melt could not pull itself together and it coated the surface.

Zn170 was grown under the identical conditions used for Zn169. The substrate was from a lot of CdZnTe that was 10 degrees off the 100 (Figures 31 and 32). Where Zn169 was only 23 microns under the same growth conditions, Zn170 was over 35 microns. Also of interest is the crystallographic appearance of the "melt back", which appears as rectangular features. If one desires to grow on orientations other than the 111 (A or B faces still need to be defined), work is needed to determine the optimum growth conditions.

Figure 50. Figure 50 is an FTIR of a HgCdTe epitaxy (Cd160) before etching off five microns from the surface. The cutoff wavelength is 4.50 microns.

Figure 51. Figure 51 is an FTIR of Cd160 after five microns were removed from the surface. The cutoff is 4.45 microns. The change in cutoff wavelength when five microns of epitaxy were removed was less than 0.005 micron, which corresponds to less than a 0.001 change in x-value composition for $Hg(1-x)Cd(x)Te$ with x=0.28 corresponding to 4.45 micron cutoff (Figure 50).

Figure 52. Figure 52 is an FTIR of HgZnTe, Zn162. The cutoff wavelength is 7.0 microns. Figures 52 to 59 illustrate the change in shape of the spectral trace. The curve becomes less sharp at longer wavelengths. This same trend is reported in the literature [9].

Figure 53. Figure 53 is an FTIR of Zn163. The cutoff wavelength is 8.3 microns.

Figure 54. Figure 54 is an FTIR of Zn169. The cutoff wavelength is 9.3 microns.

Figure 55. Figure 55 is an FTIR of Zn171. The cutoff wavelength is 7.4 microns.

Figure 56. Figure 56 is an FTIR of Zn172. The cutoff wavelength is 8.3 microns. Zn 172 was an attempt to reproduce the results

of Zn 163, which had an 8.3 micron cutoff wavelength (Figure 53).

Figure 57. Figure 57 is an FTIR of Zn173. The cutoff wavelength is 9.3 microns. Zn 173 was an attempt to reproduce the results of Zn 169, which had a 9.3 micron cutoff wavelength (Figure 53).

Figure 58. Figure 58 is an EDS analysis of Zn166. It shows the constant composition of the Hg and Zn across the epitaxy.

Figure 59. Figure 59 is an EDS analysis of Zn170. Zn170 was grown on an unfavorable orientation (10 degrees off the 100). It was a poor epitaxy.

Figure 60. Figure 60 is an EDS profile of HgCdTe, Cd125. A possible explanation for the inconsistent near surface compositions is that the microprobe analysis was too close to the surface. The analysis was performed on the cross-section of the epitaxy and, because the microprobe samples a 1 to 2 micron volume, part of the signal can be lost due to the free surface at the face of the sample when the microprobe beam is positioned too close to the edge of the sample.

Figure 61. Figure 61 is an EDS profile of HgCdTe, Cd140.

Figure 62. Figures 62 to 69 are furnace temperature profiles showing Mercury Co.'s capability to shape temperature profiles through the use of computer modeling and furnace fabrication techniques. Figure 62 is a plot of furnace #C1 with and without an epitaxy load. In this type of furnace the load affects the temperature profile. LPE of HgCdTe and HgZnTe require a flat temperature profile. Figure 62 shows a load profile that needs improvement.

Figure 63. Figure 63 shows a series of temperature profiles that occurred while the furnace thermal characteristics were being mechanically shaped. The profiles were initially centered around the 10 inch marker and were then moved to a center around the 7 inch marker.

Figure 64. Figure 64 shows an acceptable loaded furnace temperature profile for epitaxy. This flat profile shape is maintained throughout the entire processing temperature range.

Figure 65. Figure 65 shows a comparison of the modeled thermal characteristics of furnace #C2 and the radial temperatures through the furnace structure while in operation. Accurate models allow Mercury Co. to shape furnace temperature profiles in a timely and cost effective manner. More important, radical designs can be explored in a computer before expensive resources are committed. Once a new design is chosen and the furnace becomes operational, the models can be modified to take into account subsequent data.

Figure 66. Figure 66 is a thermal profile of the multi-zone B-series prototype furnace. The B-series furnaces have a unique non-symmetrical design that gives a more symmetrical temperature profile than most symmetrical designs.

Figure 67. Figure 67 is a series of temperature profiles showing the thermal shaping capabilities of the #B1 furnace. Furnace #B1 was designed to process 10 x 13 mm wafers. Small wafers require only a two to three inch flat temperature zone.

Figure 68. Figure 68 shows two thermal processing profiles used in furnace #B1 during this program.

Figure 69. Figure 69 is a plot showing the advanced thermal capabilities of the production epitaxy furnace, #B2. The natural profile of the furnace has a flat ten inch zone. The modified profile above the flat profile shows that the end zones can be adjusted without affecting the center zones.

Figure 70. Figure 70 is a pictorial summary of substrates and epitaxies developed during this project. Starting at the lower left, mounted on the glass for polishing are Cd(0.8)Zn(0.2)Te slices. They are 10 degrees off the 100 and were used for chemical analysis, x-ray diffraction for lattice spacing determination and initial HgZnTe LPE growth conditions determination. The plate on the right is the same material after low damage mechanical polishing.

The wafer at the top left is an "as received" Galtech Cd(0.8)Zn(0.2)Te wafer. The wafers had excellent orientation and surface polish. The wafers arrived with a protective plastic covering.

The second wafer from the left is ready for LPE.

The third wafer from the left was a great success even though it looks bad. Analysis of the problems at this stage led to the success of the next wafer.

The fourth wafer from the left, Zn166, was broken so several analyses could be performed on the two sides.

The last two wafers are Zn168 and Zn169, respectively. Not shown are Zn171, 172, and 173. They look the same as Zn168 and Zn169.

Figure 71 is the mandatory reflection of the company name in epitaxy picture.

Figure 72. Figure 72 shows the results of a cost study performed by Mercury Co.

Figure 73. Figure 73 is a table with the cutoff wavelengths adjusted for temperature for given x-values.

Figure 1. IBAS equipment located at ETC.
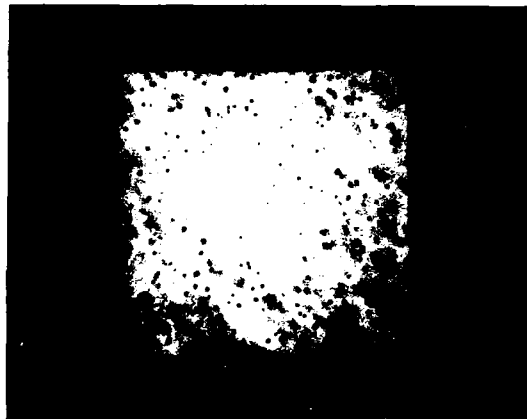
Figure 2. 50x IR of CdZnTe showing 243 precipitates.

Figure 3. Contrast enhancement of cellular structure.
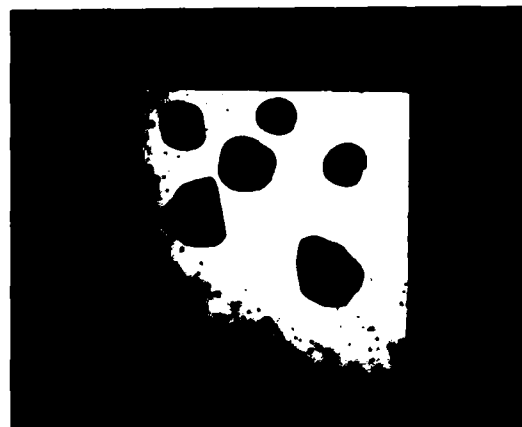
Figure 4. Discrimination process.
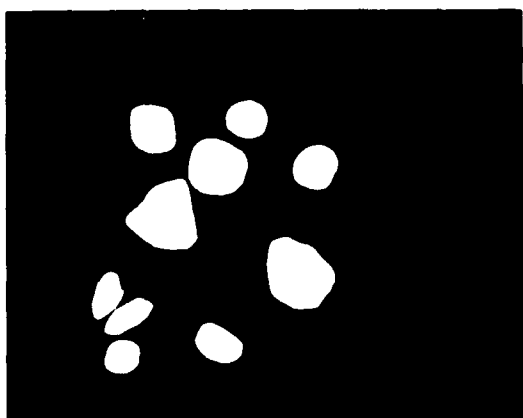
Figure 5. Erosion process.
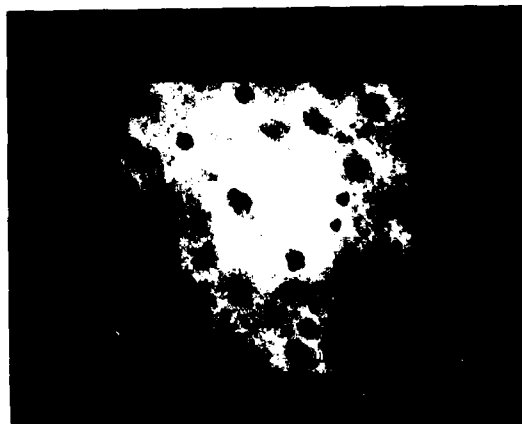
Figure 6. 400x illustrating 6 micron triangular features.

Figure 7. IR micrograph
of Cd(0.8)Zn(0.2)Te.
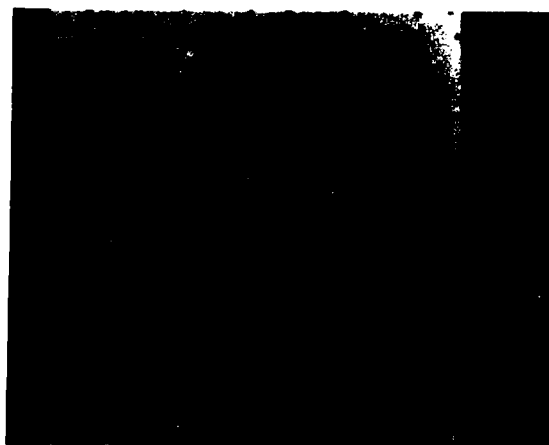
Figure 8. Figure 7 enhanced,
showing cellular distribution.
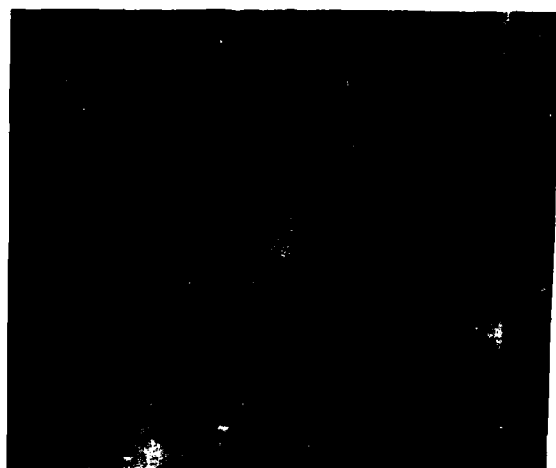
Figure 9. 400x showing
triangular shaped particles.
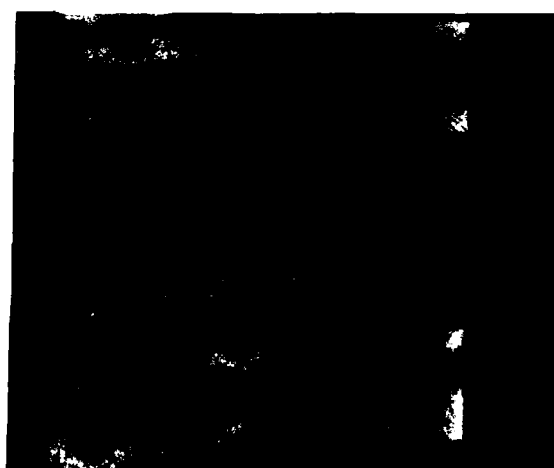
Figure 10. 800x; particles
arranged on a tetrahedral.

Figure 11. 400x of another
group; triangular particles.
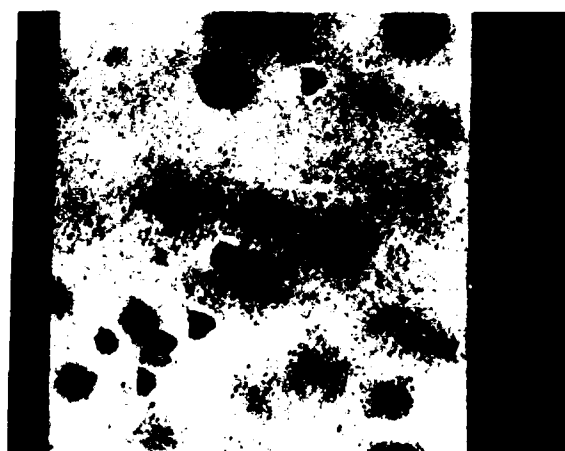
Figure 12. 800x illustrating
6 micron triangular features.
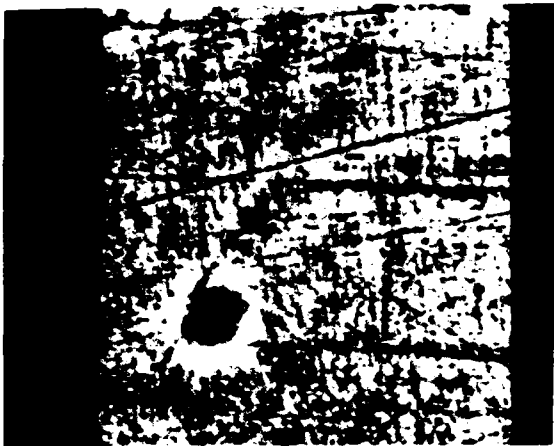
Figure 13. IR surface analysis of CdZnTe.
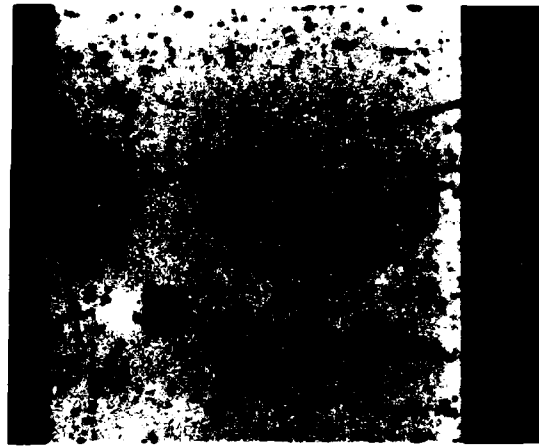
Figure 14. Figure 13 enhanced, removing scratches from image.

Figure 15. Denuded region at a grain boundary.

Figure 16. Particle analysis of a defined volume.
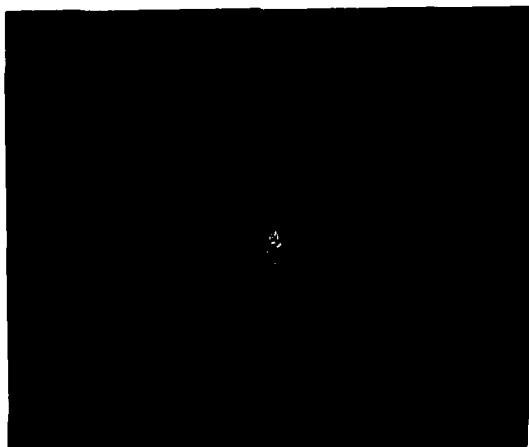
Figure 17. 400x image of the enclosed region of Figure 16.
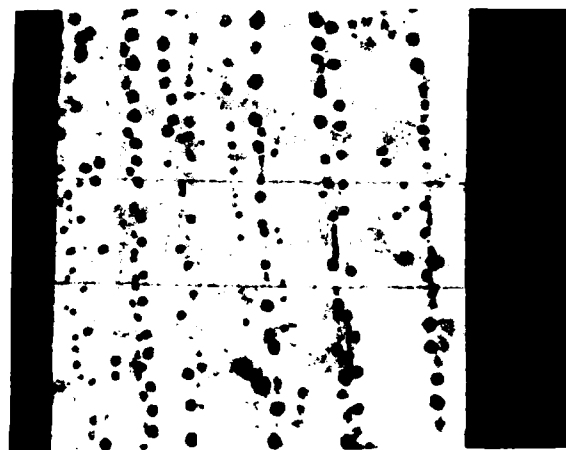
Figure 18. Processed image showing planar analysis.
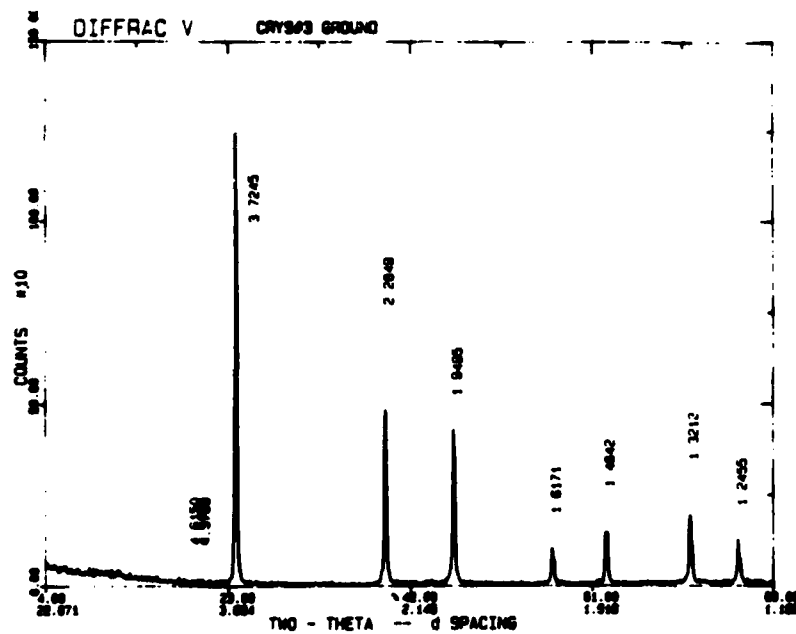
Figure 19. X-ray powder diffraction analysis of CdTe; 6.4510 Angstrom lattice spacing.
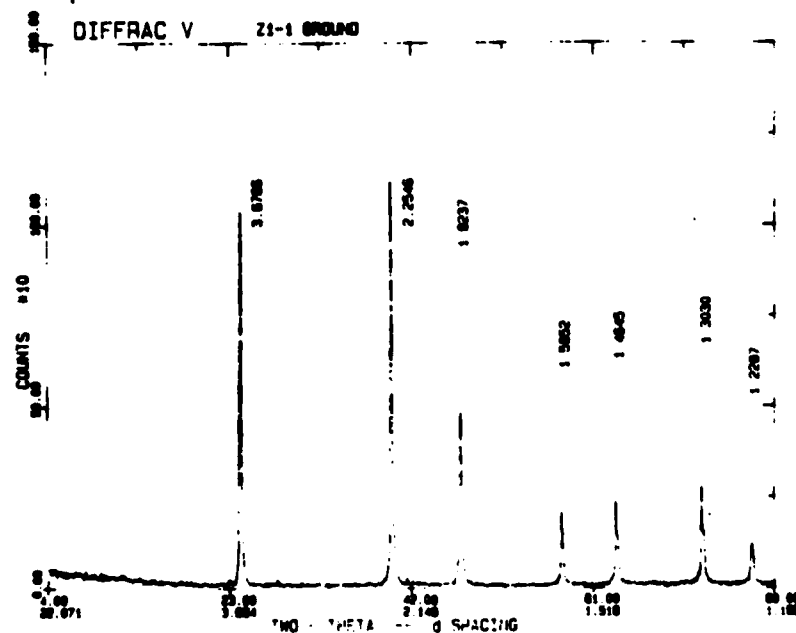
Figure 20. Cd(0.8)Zn(0.2)Te; 6.3681 Angstroms lattice spacing which is 1.3% less than CdTe.

- 52 -
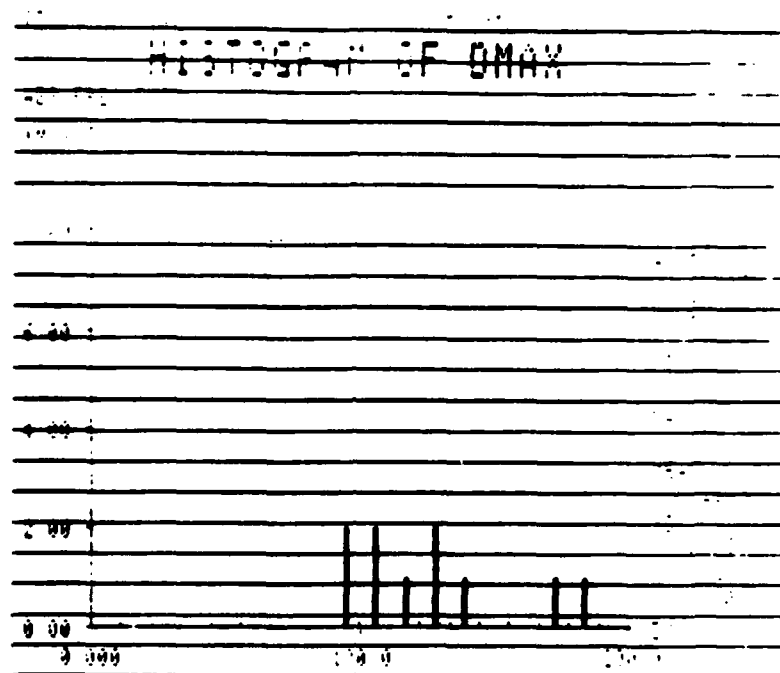
Figure 21. Diameter distribution (in microns) of
the cellular regions shown in Figures 2 through 4.
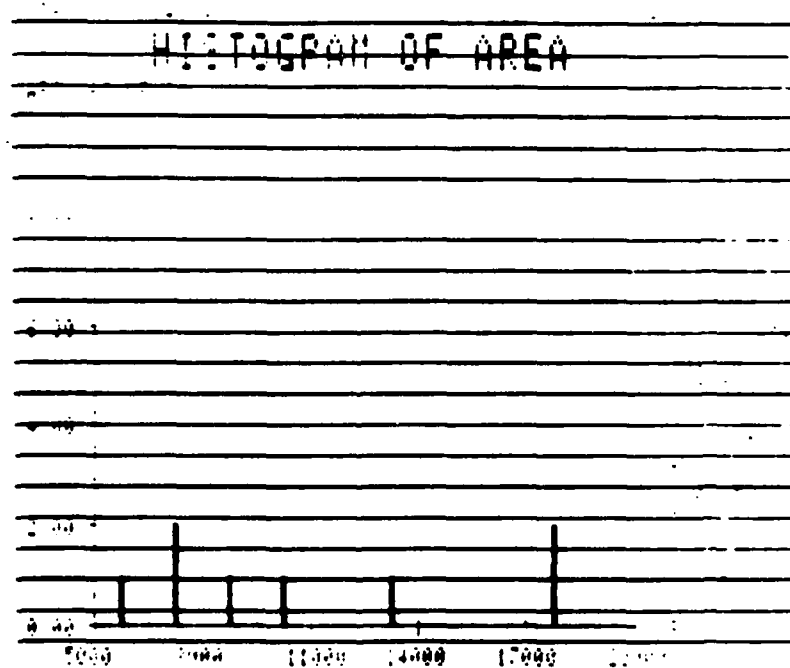
Figure 22. Cross-sectional area (square microns)
of the cellular objects shown in Figure 4.

- 53 -
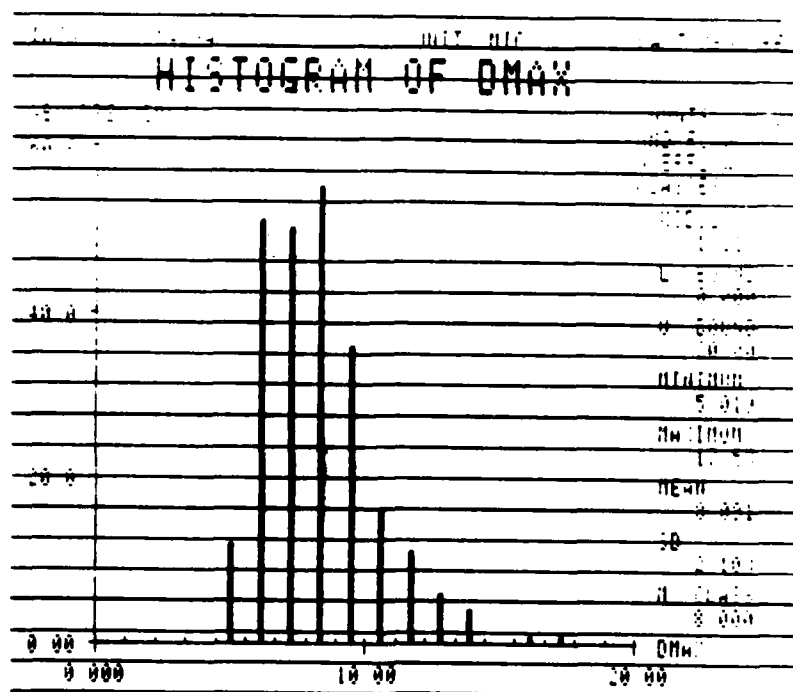
Figure 23. Diameter distribution (in microns) of the 243 particles shown in Figure 2.
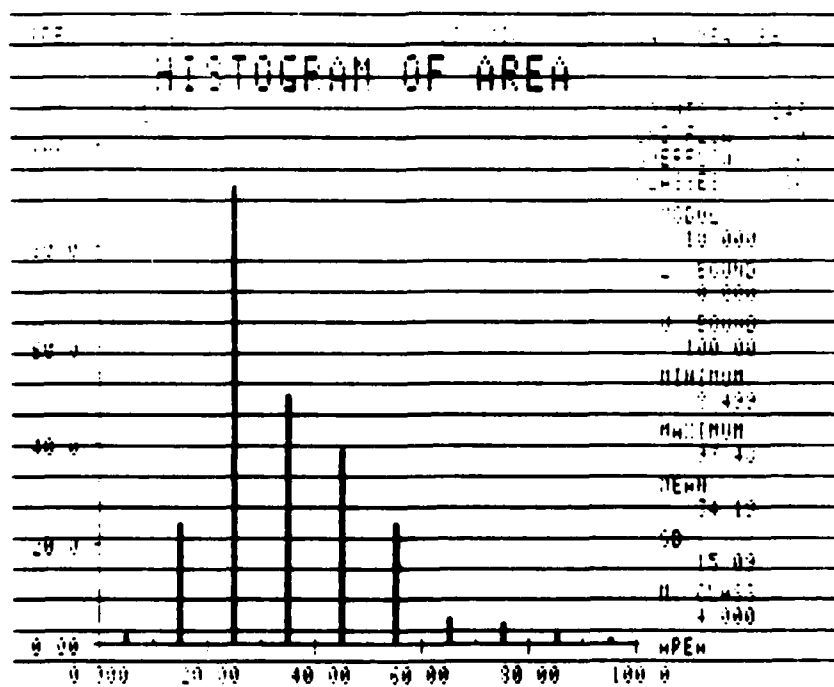
Figure 24. Cross-sectional area (square microns) of the particles shown in Figure 2.
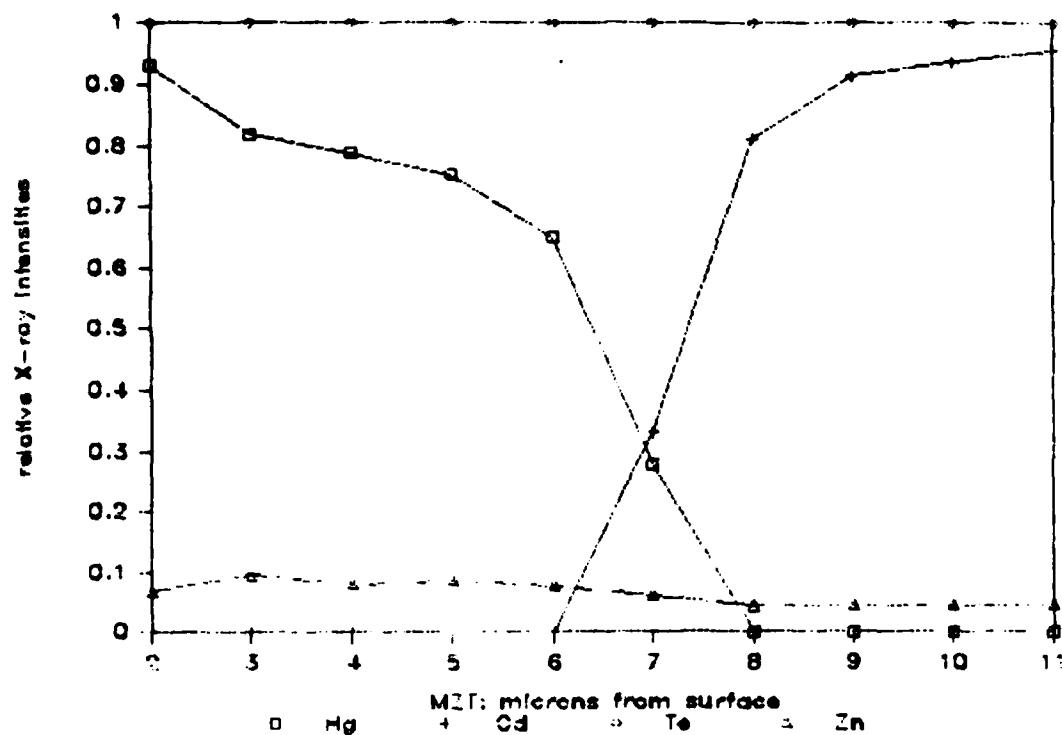
Figure 25.   Relative x-ray intensities using EDS across eight micron thick HgZnTe layer Zn165.
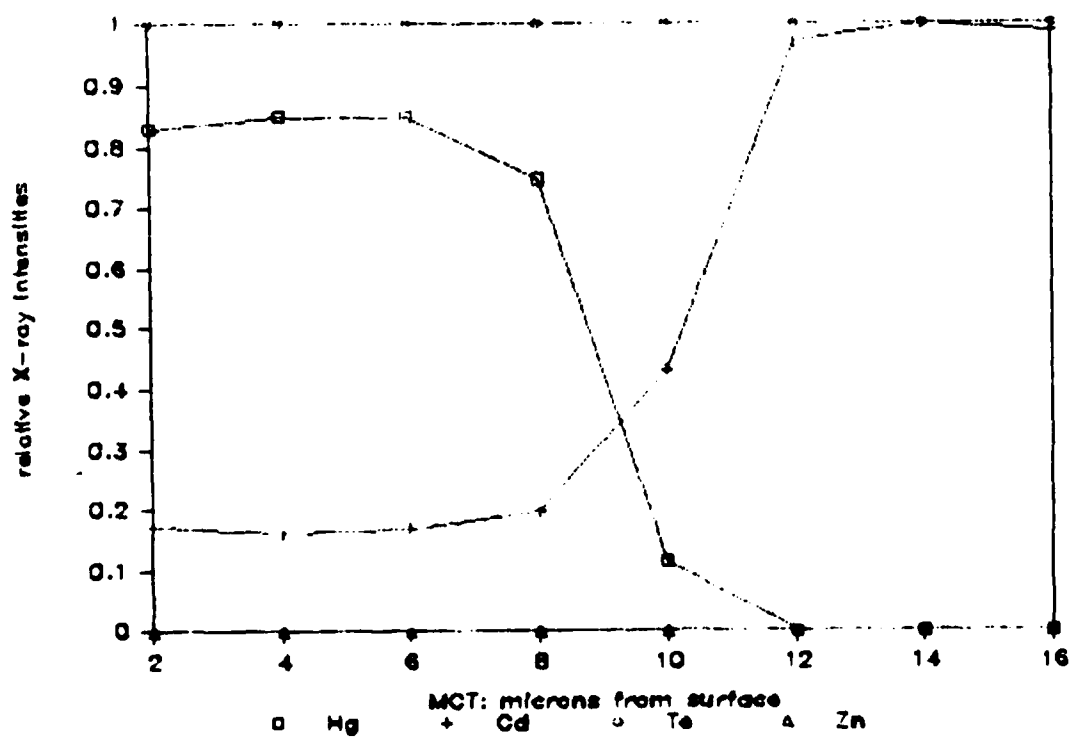
Figure 26. Relative intensity EDS plot for HgCdTe on a CdTe substrate.
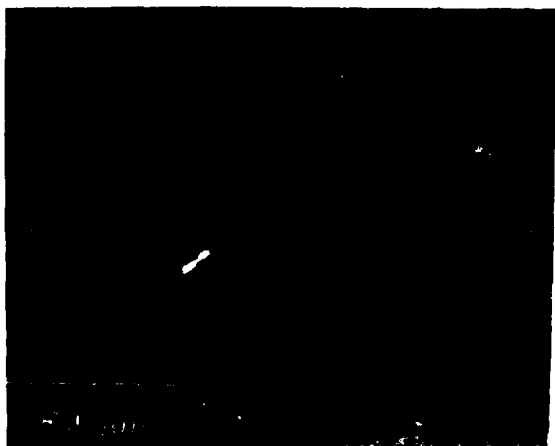
Figure 27. SEM of CdZnTe showing an unknown defect.

Figure 28. Electron channeling pattern; 100 orientation.

Figure 29. TEM of CdZnTe.
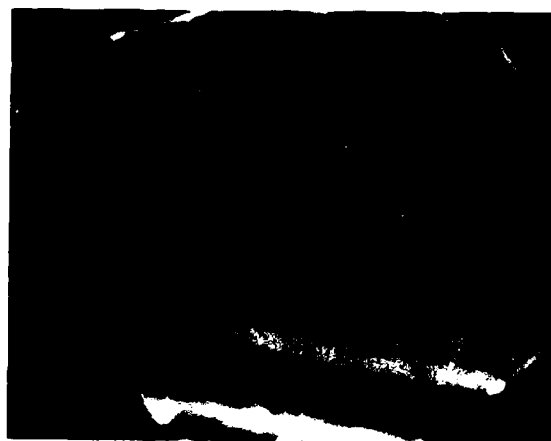
Figure 30. Kikuchi lines in a TEM diffraction pattern.
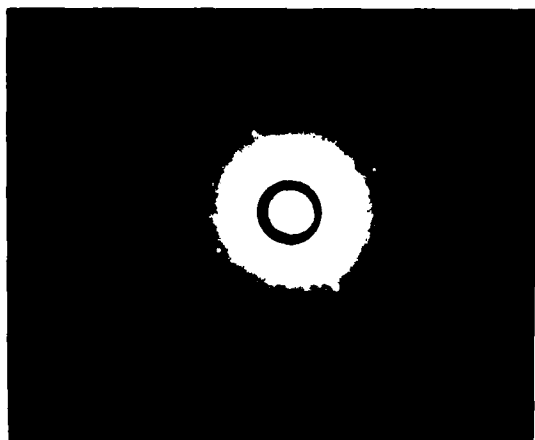
Figure 31. Laue x-ray showing 10 degrees off the 100.
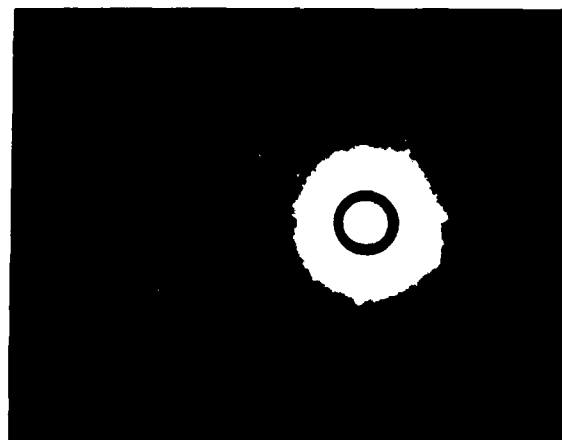
Figure 32. Laue x-ray after tilting sample ten degrees.
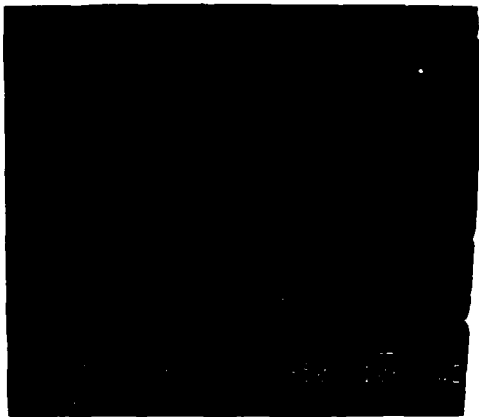
Figure 33. SEM of 30 micron
thick HgCdTe epitaxy.

Figure 34. 500x calibration;
each division = 10 microns.

Figure 35. 500x HgZnTe,
20 microns thick; Zn166.

Figure 36. A SEM showing the
EDS positions of measurement.
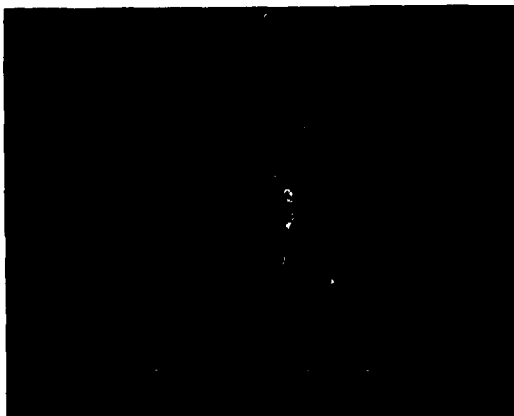
Figure 37. SEM showing defects
that had to be eliminated.

Figure 38. The defects were
determined: Hg tellurides.

Figure 39. SEM of Te rich
HgTe tip of defect on Zn166.
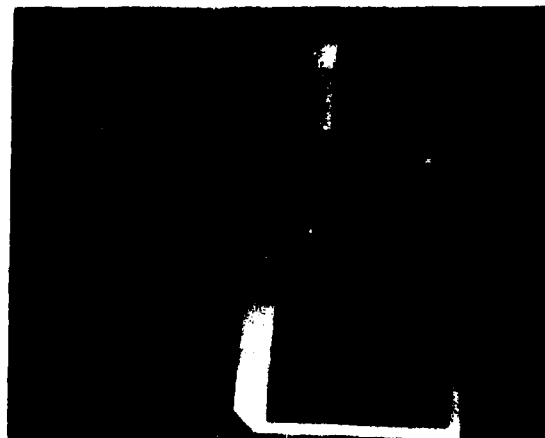
Figure 40. HgZnTe Zn168, 166
and epitaxial analyses.

Figure 42. 100x of Zn 168
showing a large defect.
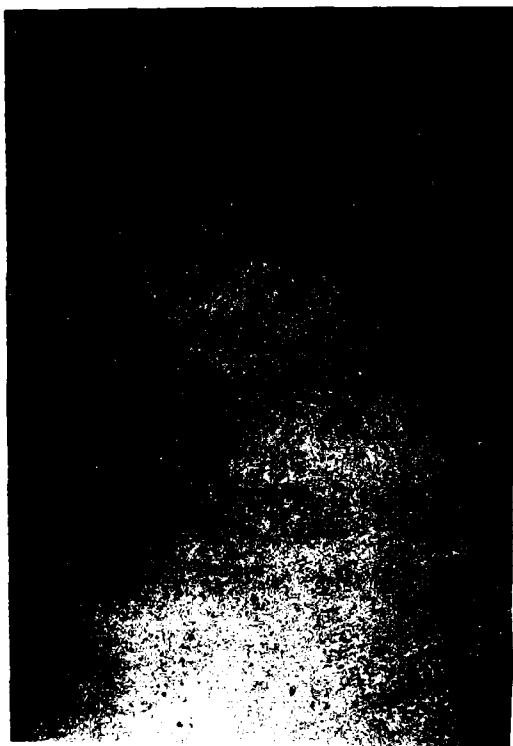
Figure 41. 50x showing 1cm
area at edge of Zn168.

Figure 43. 500x illustrating
platelet pinning.
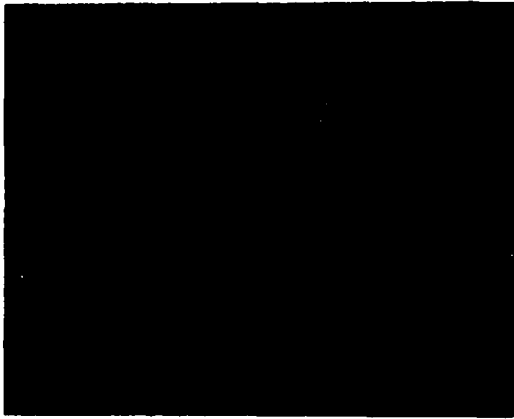
Figure 44. 25x micrograph of the largest defect area.
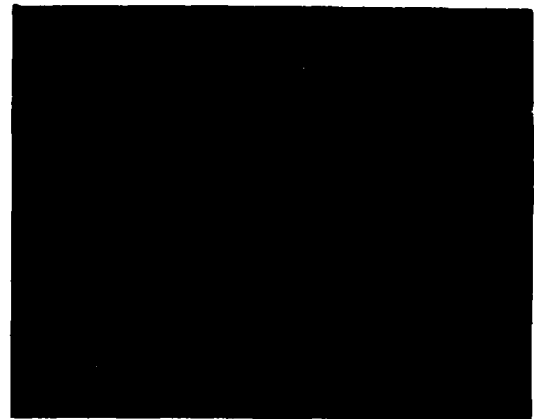
Figure 45. 100x illustrating triangular growth platelets.
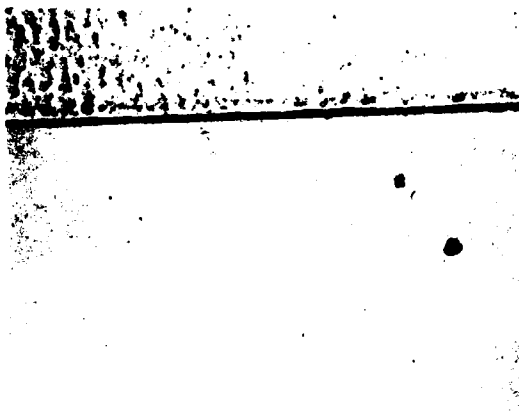
Figure 46. 100x of Zn162. All areas are same height.

Figure 47. 100x; Zn169. Twin grew 20% faster.

Figure 48. 500x; Zn168. The twin has more defects.

Figure 49. 500x; Zn170. 35 micron poor HgZnTe epitaxy.
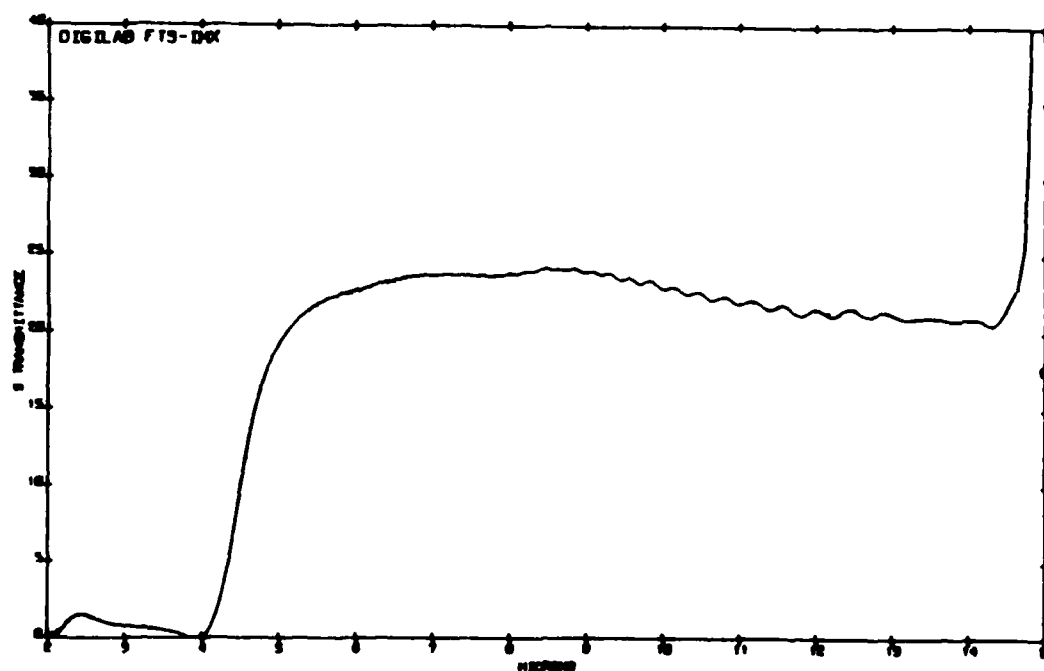
Figure 50. Cd160; HgCdTe, cutoff wavelength of
4.50 microns before etching.
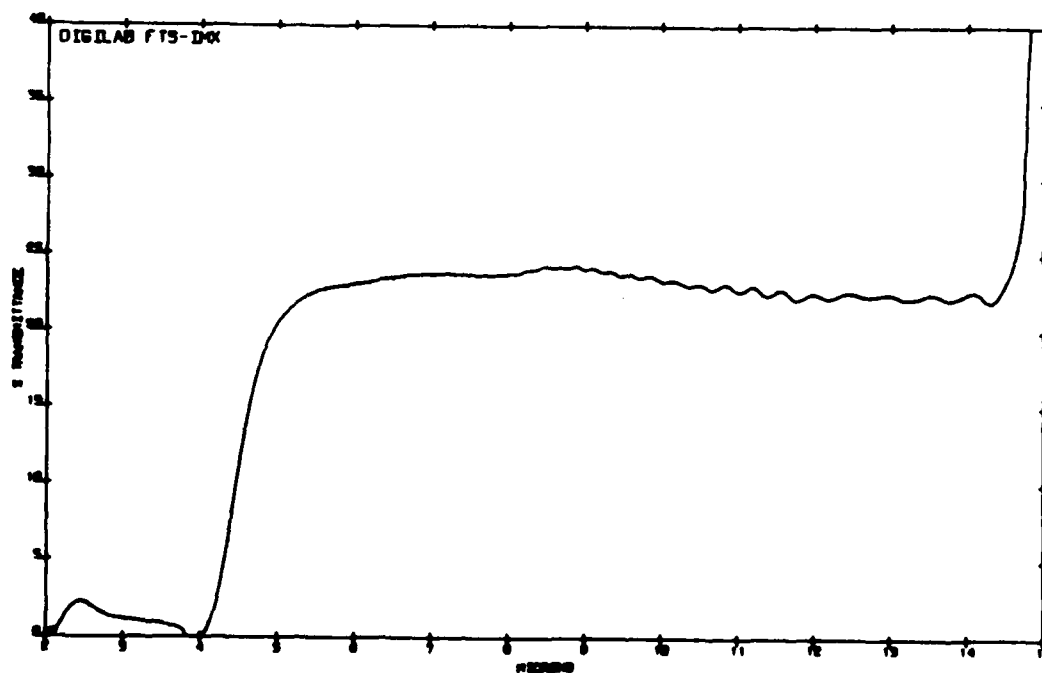
Figure 51. Cd160; after five microns of epitaxy
were removed.

- 60 -
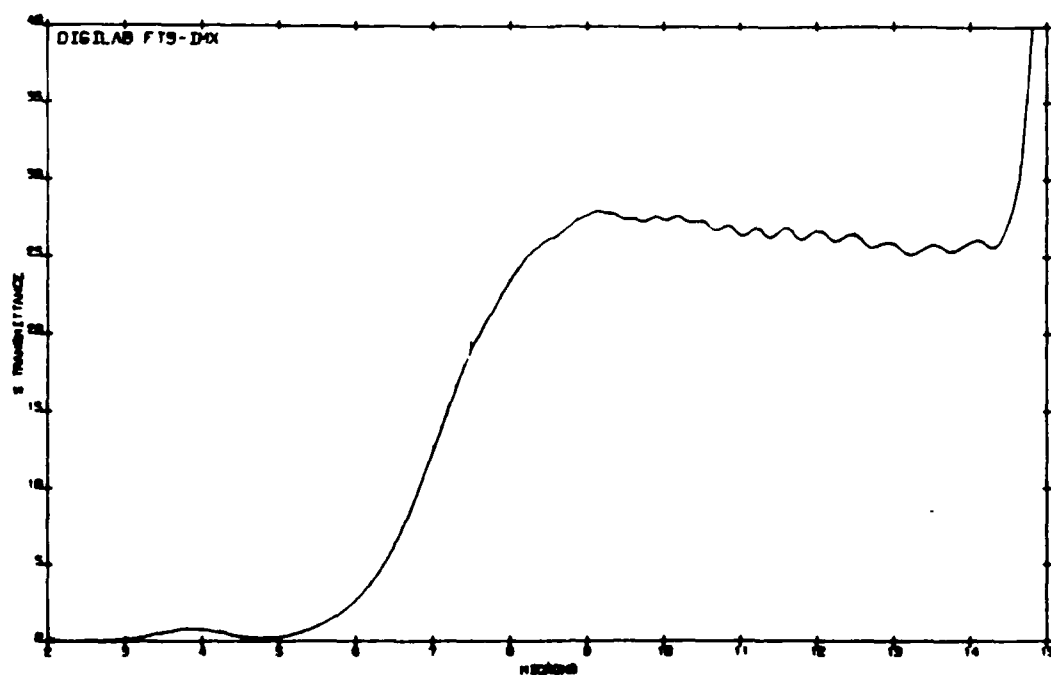
Figure 52. Zn162; HgZnTe with a 7.3 micron room
temperature cutoff wavelength.
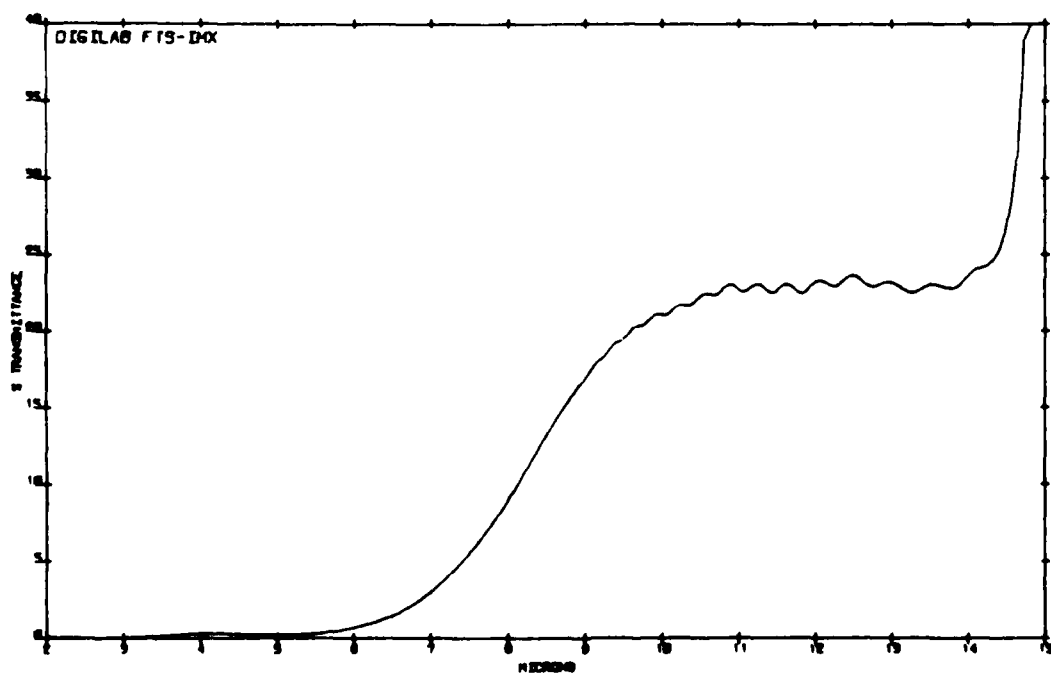
Figure 53. Zn163; 8.5 micron room temperature
cutoff wavelength.
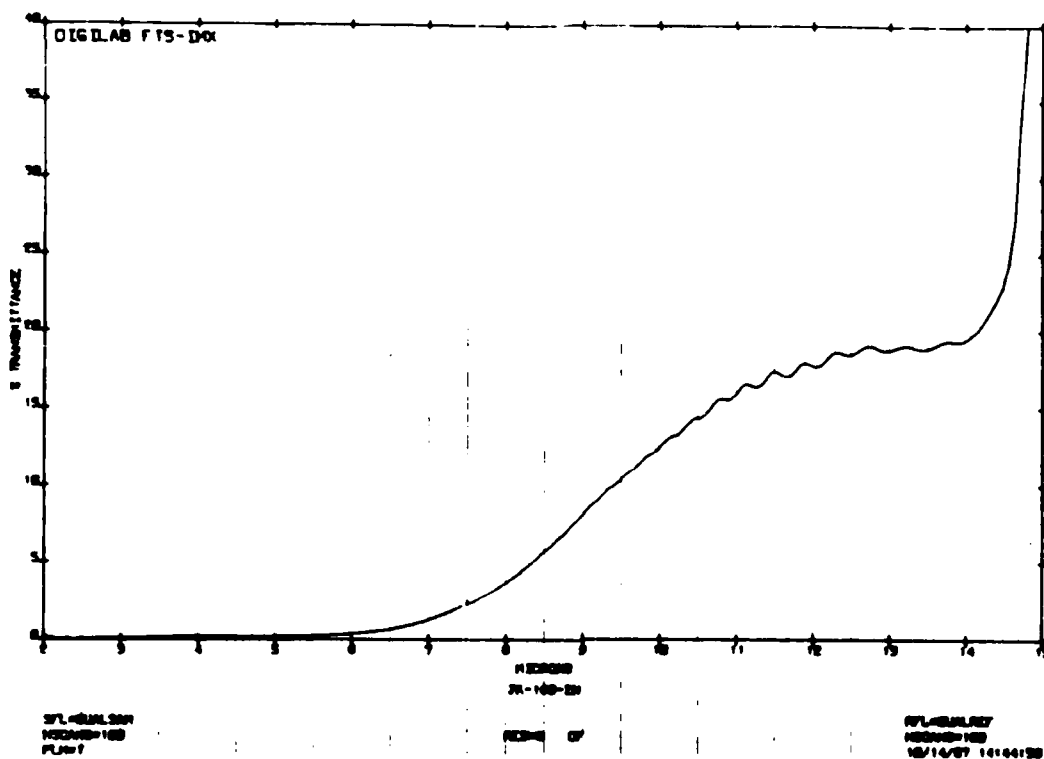
Figure 54.   Zn 169; 9.3 micron cutoff wavelength.
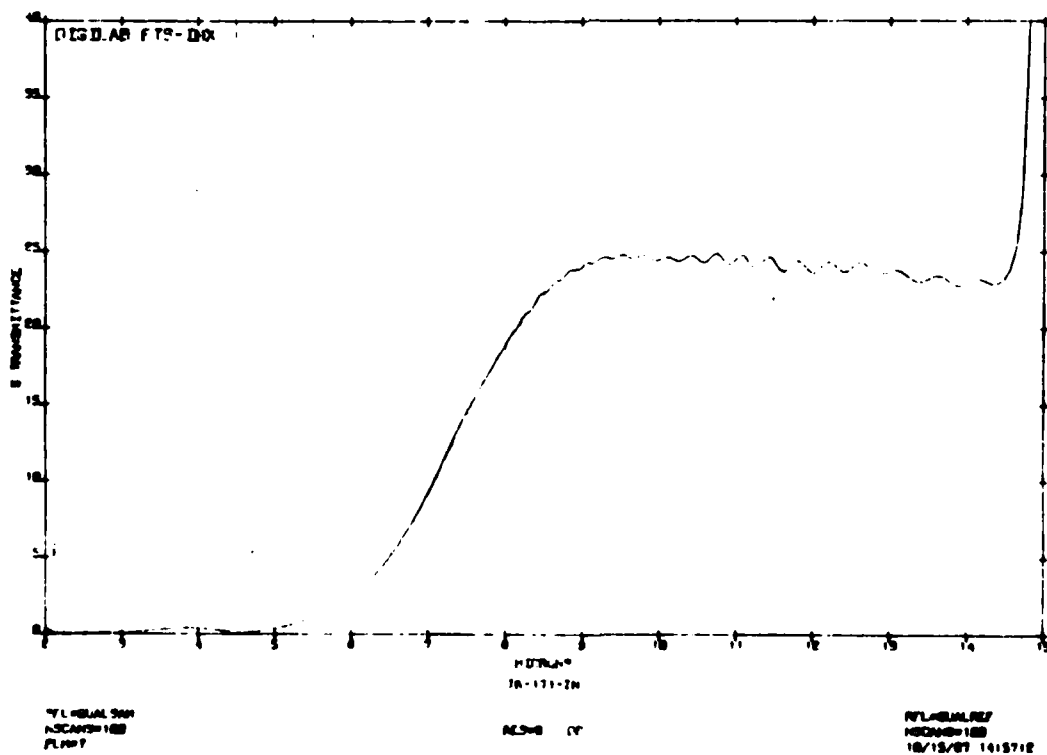
Figure 55.   Zn171; 7.3 micron cutoff wavelength.
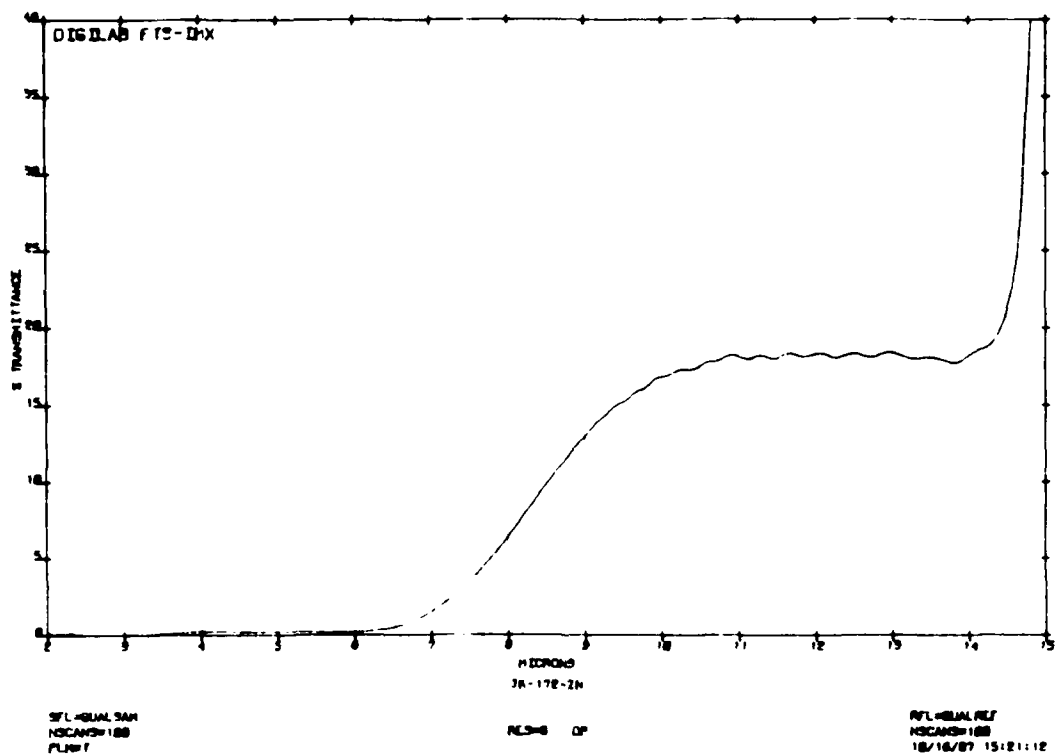
Figure 56.   Zn 172; 8.5 micron cutoff wavelength.
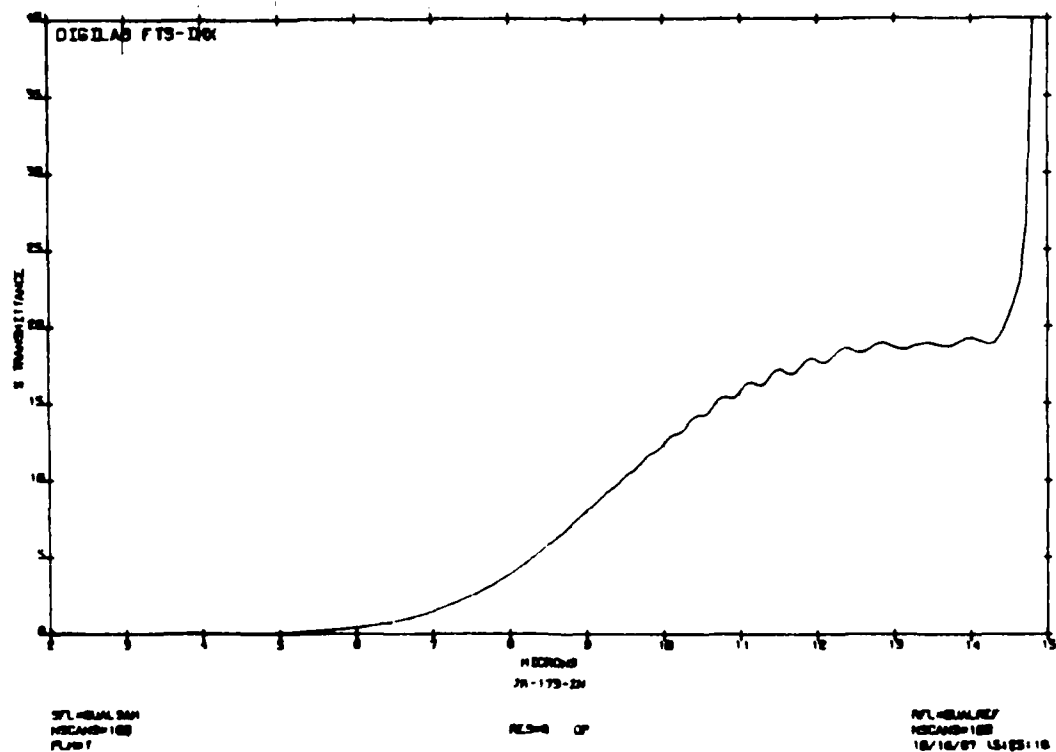
Figure 57.   Zn173; 9.3 micron cutoff wavelength.
This was a successful attempt to reproduce Zn169.
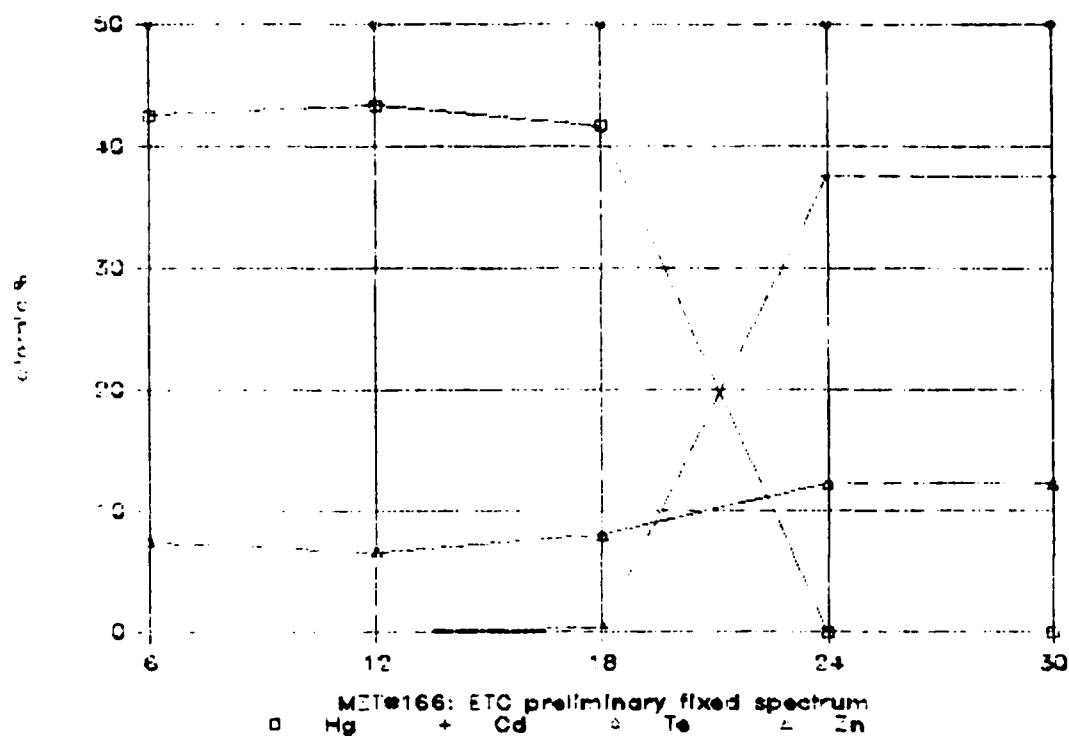
Figure 58. EDS analysis of Zn170 showing the
constant Hg and Zn composition across the layer.
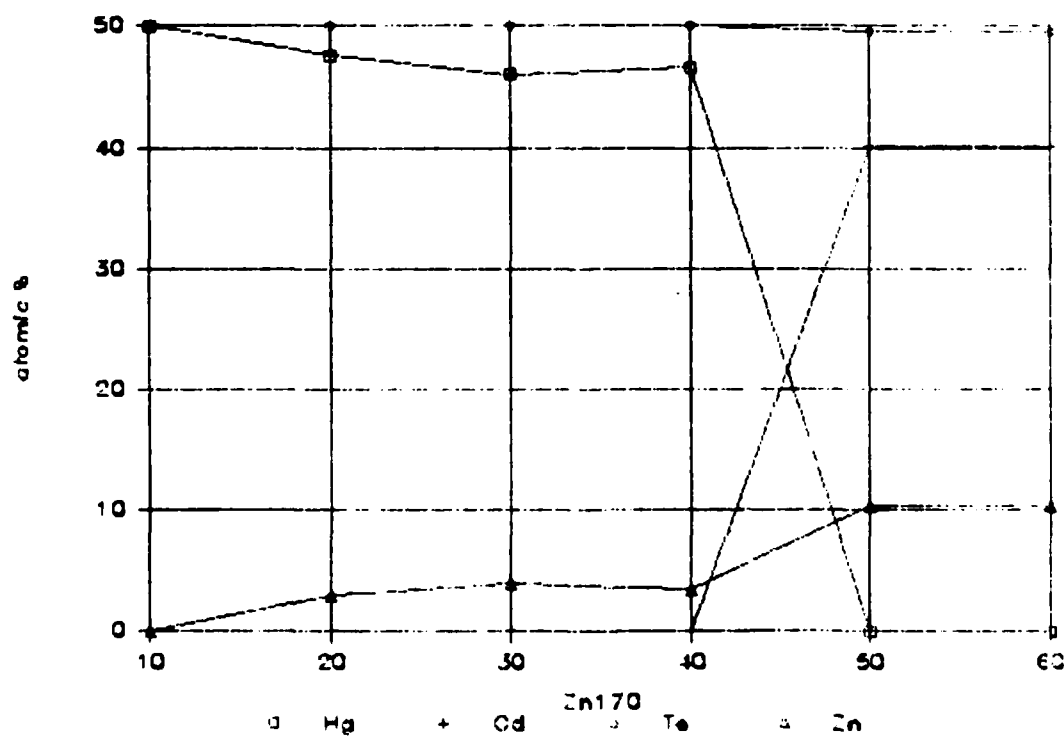
Figure 59. EDS of Zn170; a poor epitaxy due to
unfavorable orientation.
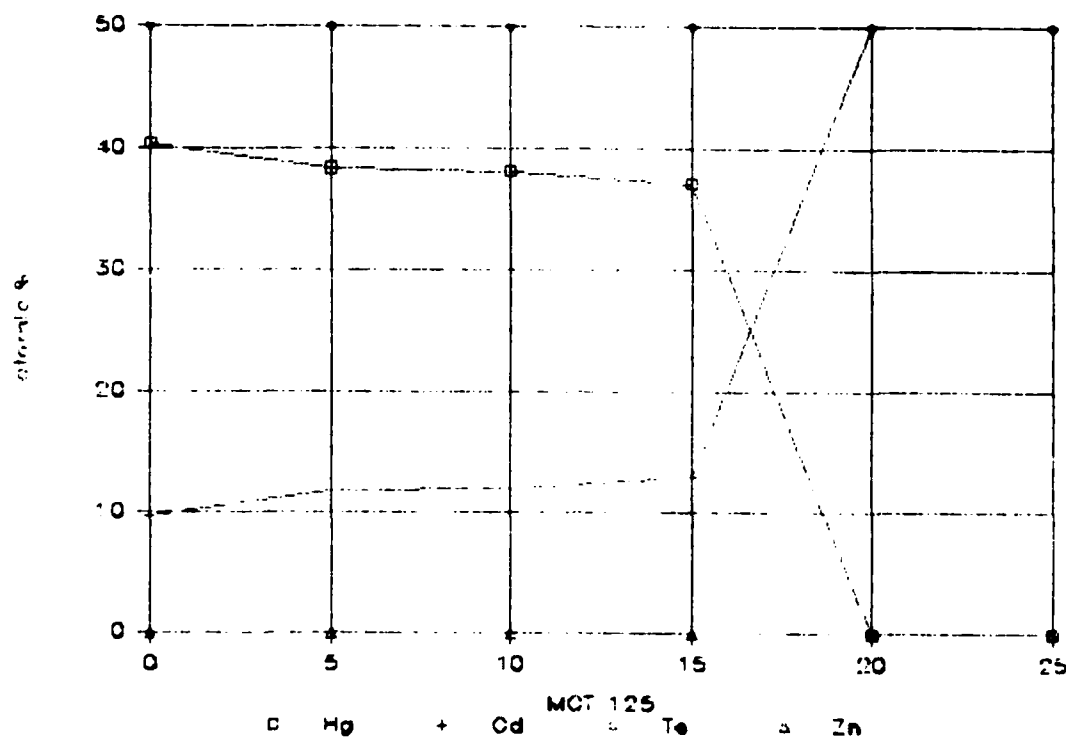
Figure 60. EDS analysis of Cd125, HgCdTe.
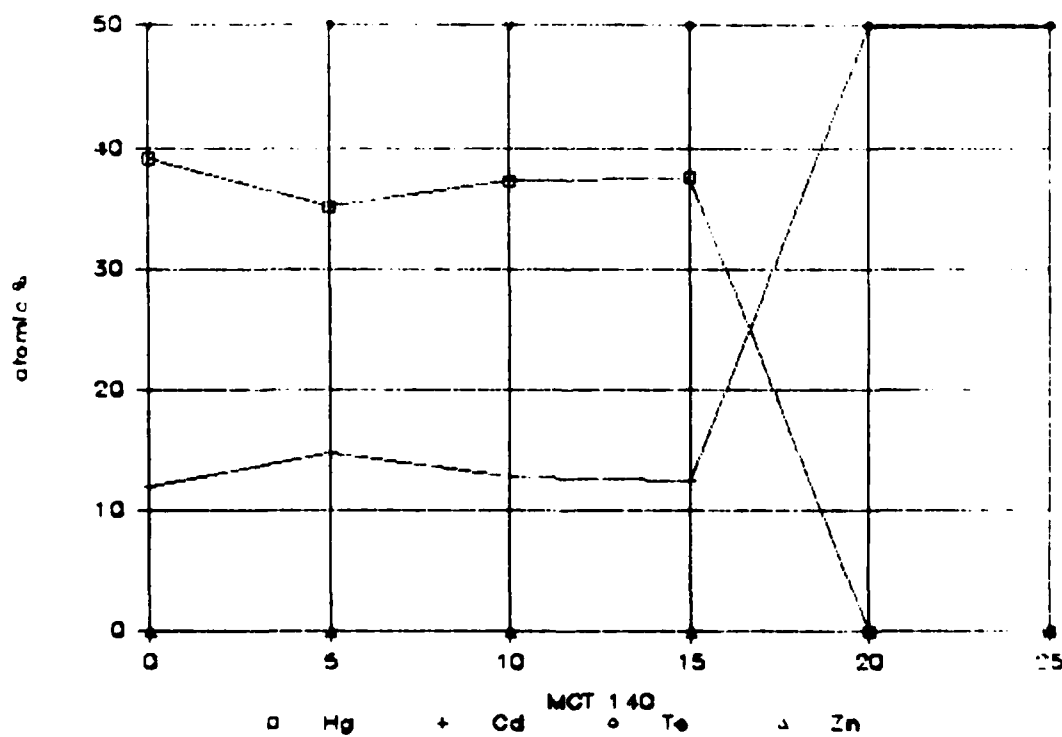
Figure 61. EDS of Cd140, HgCdTe showing uniform
Hg and Cd compositon across the layer.
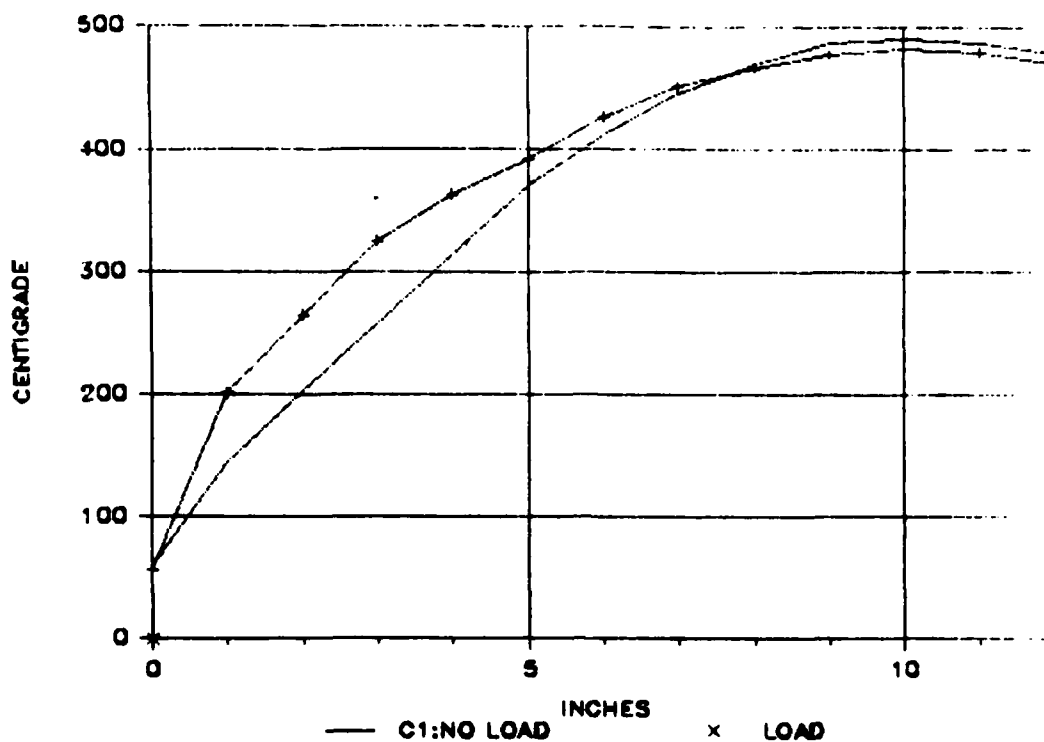
Figure 62. Temperature profiles of furnace #C1 showing how an epitaxy load affects the profile.
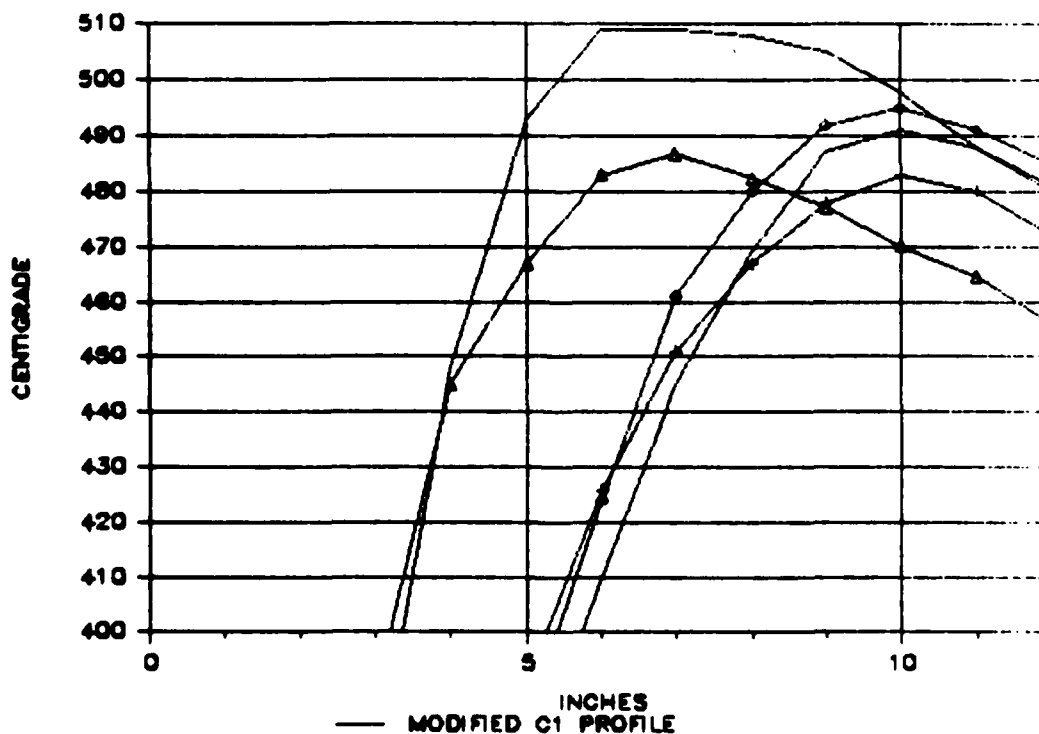
Figure 63. Furnace #C1 temperature profiles that occurred while mechanically shaping the profile.
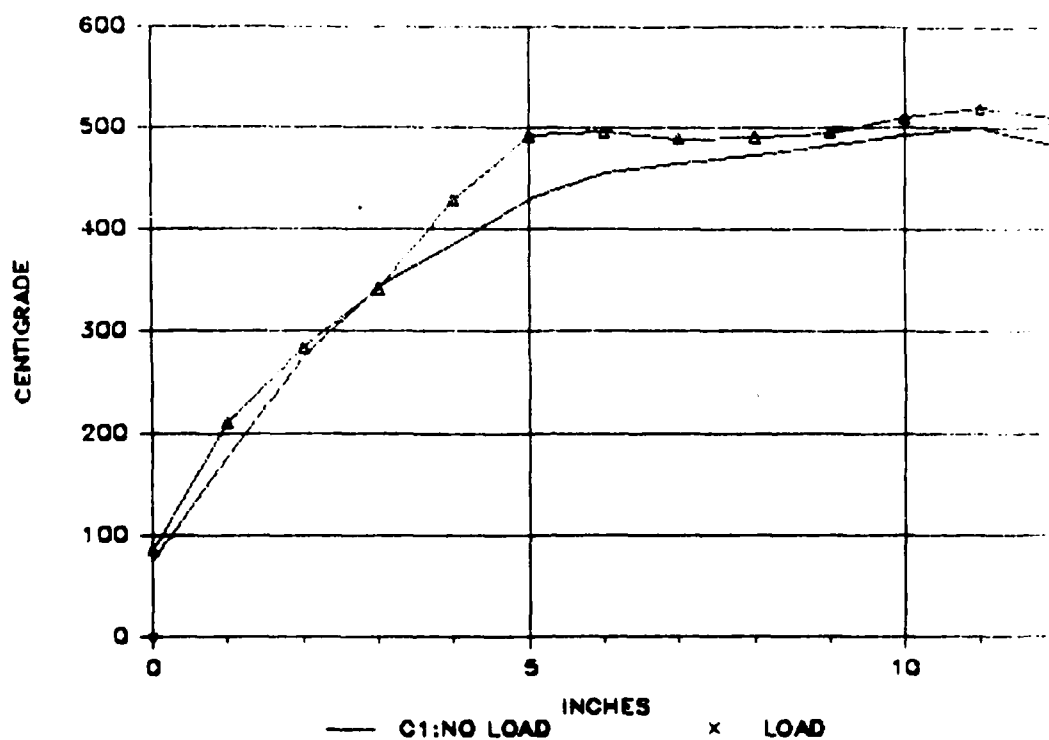
Figure 64. Furnace #C1 with an acceptably flat temperature suitable for epitaxy.
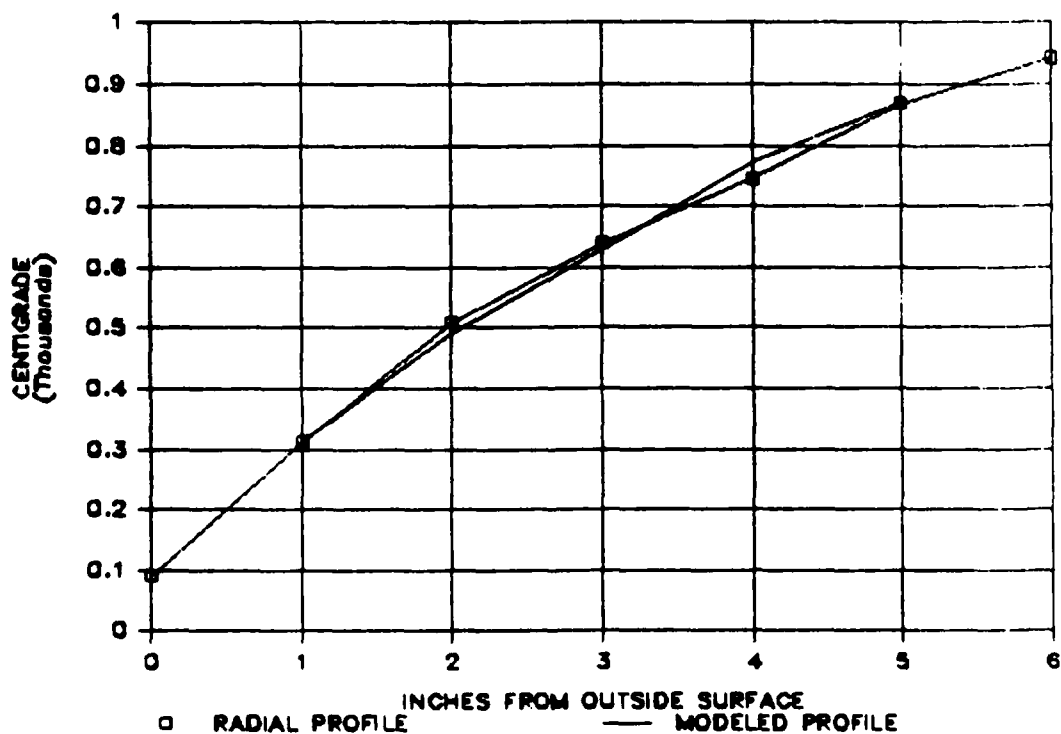
Figure 65. Comparison of the modeled vs. operational temperatures through the furnace structure.
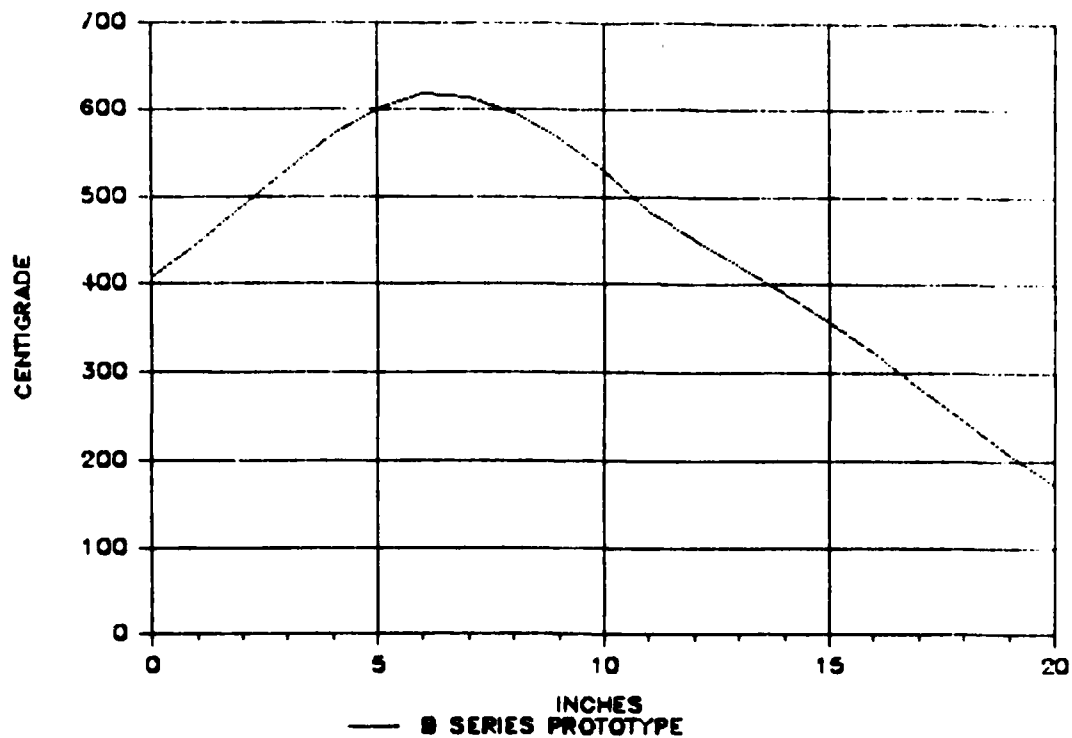
Figure 66. Temperature profile showing the
symmetric temperature distribution in the
non-symmetrically designed B-series furnaces.
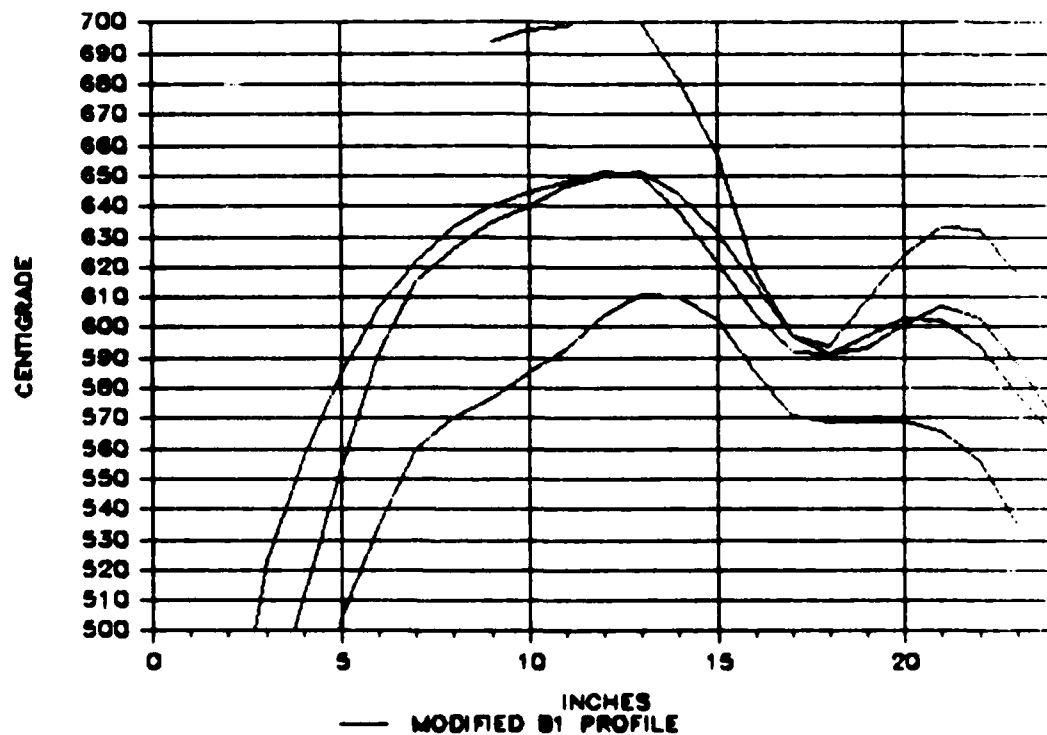
Figure 67. Thermally shaping the #B1 furnace
for a three inch flat zone to process 1cm parts.

- 68 -
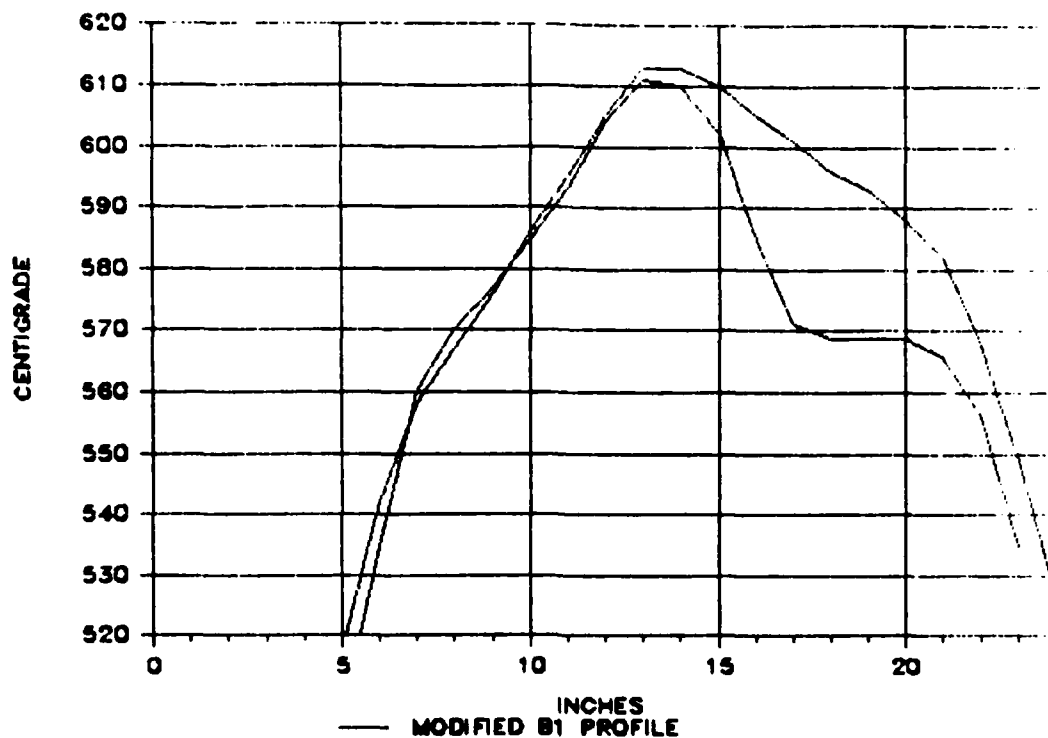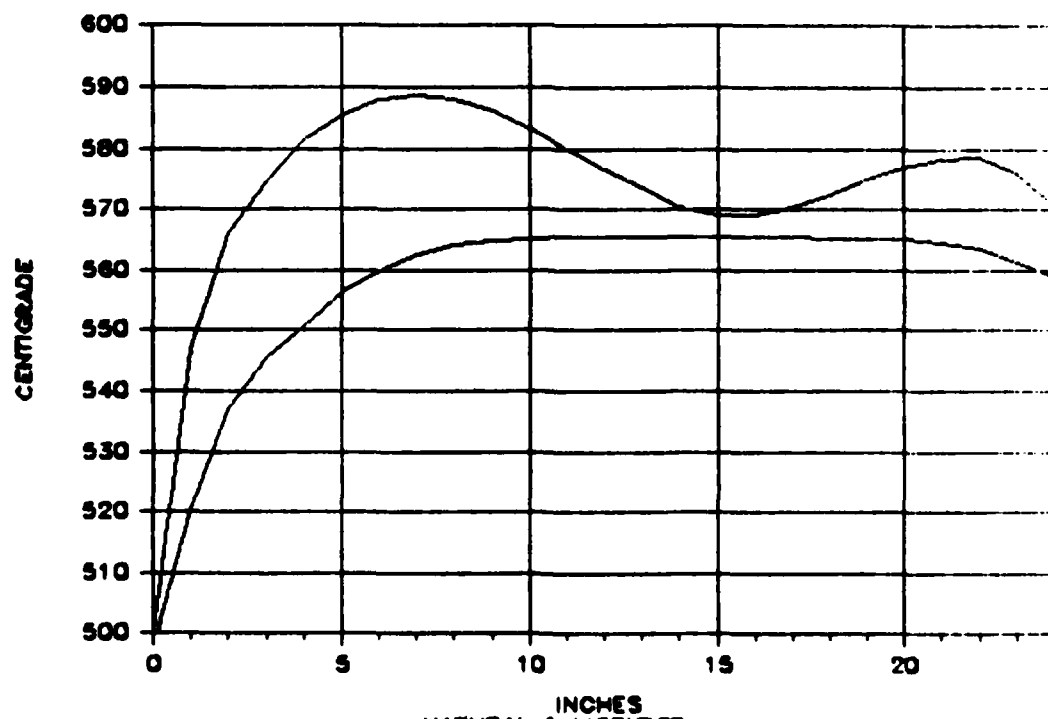
Figure 68. Two thermal processing profiles used in furnace #B1.

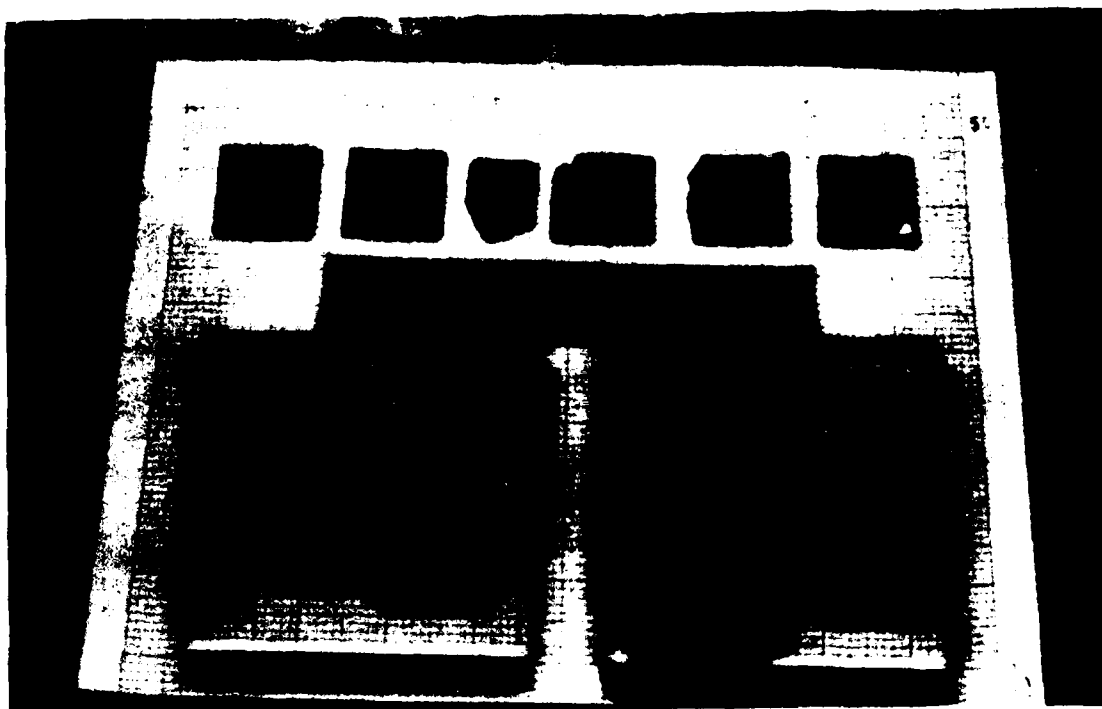Figure 69. Temperature profiles of the advanced production furnace #B2, showing ten inch flat zone.

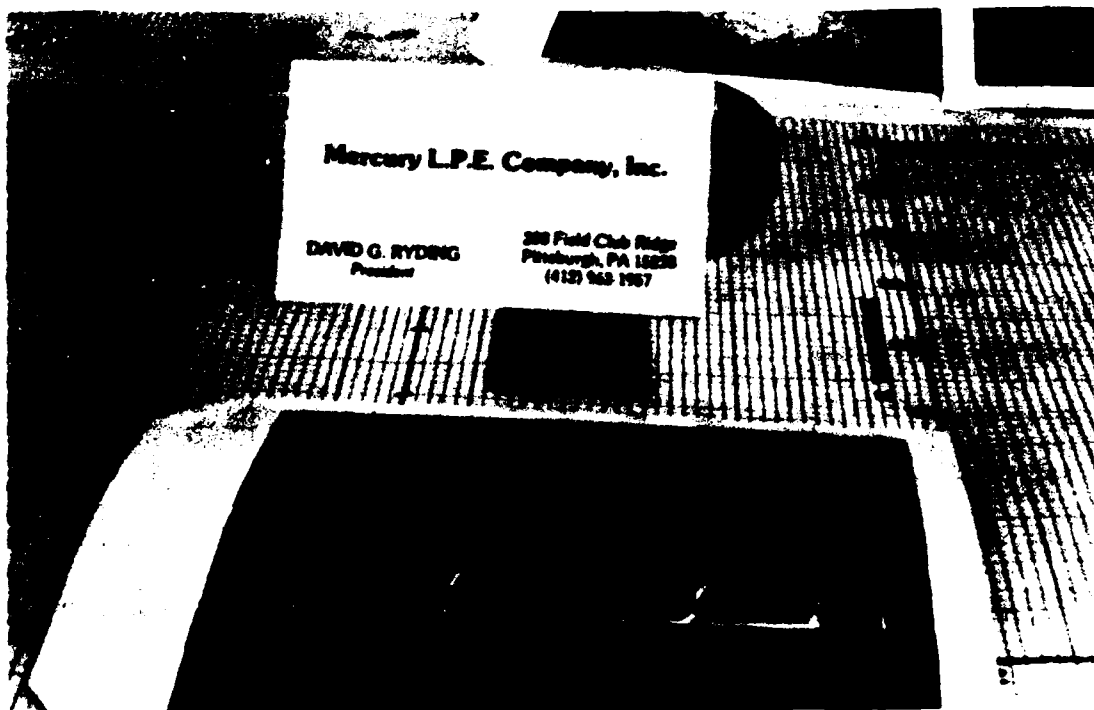Figure 70. Pictorial summary of the Cd(0.8)Zn(0.2)Te and longwave HgZnTe epitaxy development program.

Figure 71. The mandatory reflection of the company name in epitaxy picture; #Zn168, longwave HgZnTe.

The following tentative price schedule demonstrates the cost effective high volume epitaxy capability of Mercury Co.

EPIs/YR	PRICE/EPI	
100	$2,500	This scenario is for 9 sq cm HgCdTe on CdTe wafers. It is envisioned that Galtech will
200	$2,400	supply 9 sq cm and larger size wafers.
500	$2,300	
1000	$2,100	Similar pricing is anticipated for longwave HgZnTe/CdZnTe.
2000	$1,900	
5000	$1,500	
10000	$1,200	sq cm price is less than $100
20000	$1,000	

Note: these prices include the cost of the CdTe substrate. Alternate substrates could reduce the price per sq cm.

Figure 72.

Cutoff wavelength (microns)
as a function of x-value and temperature

	Temperature (degrees K)					
x	77	125	165	192	200	300
0.150	124.91	42.80	27.65	22.32	21.11	12.60
0.155	67.50	33.42	23.53	19.61	18.68	11.77
0.160	46.26	27.42	20.47	17.48	16.76	11.04
0.165	35.20	23.25	18.12	15.78	15.19	10.39
0.170	28.41	20.18	16.26	14.37	13.90	9.82
0.175	23.83	17.83	14.75	13.20	12.80	9.31
0.180	20.52	15.98	13.49	12.21	11.87	8.84
0.190	16.06	13.23	11.53	10.61	10.37	8.05
0.200	13.20	11.29	10.07	9.39	9.20	7.38
0.210	11.21	9.85	8.94	8.42	8.27	6.82
0.220	9.74	8.73	8.04	7.63	7.52	6.34
0.240	7.73	7.13	6.69	6.43	6.36	5.56
0.260	6.40	6.02	5.74	5.56	5.51	4.95
0.280	5.47	5.22	5.02	4.90	4.86	4.46
0.300	4.78	4.60	4.46	4.38	4.35	4.06

Figure 73.

10.0) ADDITIONAL RESULTS

Phase I culminated in breakthroughs in the growth of HgZnTe LPE on lattice matched CdZnTe substrates. X-ray rocking curve measurements indicate that Mercury Co.'s HgZnTe LPE has better crystal properties than that of HgZnTe reported in the literature. The HgZnTe epitaxy measurements are comparable to the best HgCdTe grown. This is important because it has been demonstrated that HgZnTe may be superior to HgCdTe. Mercury Co. is the first to report capability of producing large area HgZnTe.

Another achievement of Phase I was Galtech's development and delivery of large area, high quality, lattice matched for HgZnTe, $Cd(.8)Zn(.2)Te$ substrates. The $Cd(.8)Zn(0.2)Te$ ingot was only the second of this composition grown by Galtech. Narrow beam x-ray rocking curve measurements varied from 19 to 32 arc seconds and broad beam x-ray rocking curve measurements varied from 60 to 80 arc seconds. These measurements indicate that Galtech has a potentially important crystal growing process for the fabrication of substrates for HgZnTe.

Large area (30mm x 30mm) longwave HgZnTe grown on Galtech's substrates had narrow beam x-ray rocking curves of 50 to 80 arc seconds and broad beam x-ray rocking curves of 60 to 100 arc seconds. The variations in the epitaxy appear to follow the substrate, indicating that as the substrate improves, the epitaxy will improve.

Mercury Co. performed additional FTIR measurements after calibrating PARC's equipment and more favorable results were obtained. All of the epitaxies had 35% to 75% higher transmissions than previously reported. The results from the calibrated FTIR measurements are shown on pages 73-75.

Hall measurements were performed and the results are favorable. As-grown HgZnTe was p-type (10^18) at 77K and converted to n-type (2×10^15) at 30-40K after an eight hour mercury vapor anneal. A 24 hour anneal produced a higher n-type material. Immediate improvements in this already acceptable epitaxy can be achieved by upgrading the process materials. In Phase I Mercury Co. was interested in achieving metallurgical control of the epitaxy, rather than electrical control. When a low defect, high quality crystal structure is achieved, it will become easier to observe electrical changes due to impurities or intentional doping because crystal imperfections, which can act as self-dopants, are minimized.

The metallurgical measurements indicate that Mercury Co.'s HgZnTe has better lattice perfection, while the Hall measurements indicate comparable electrical characteristics to HgZnTe reported in the literature. The HgZnTe epitaxy measurements are comparable to the best HgCdTe grown.
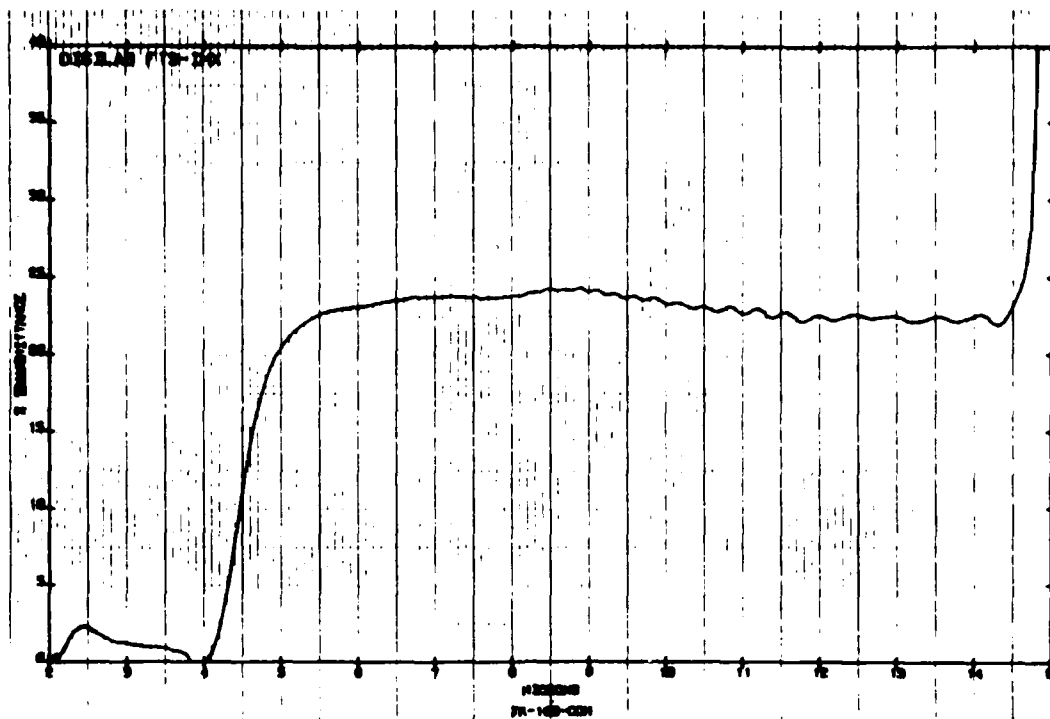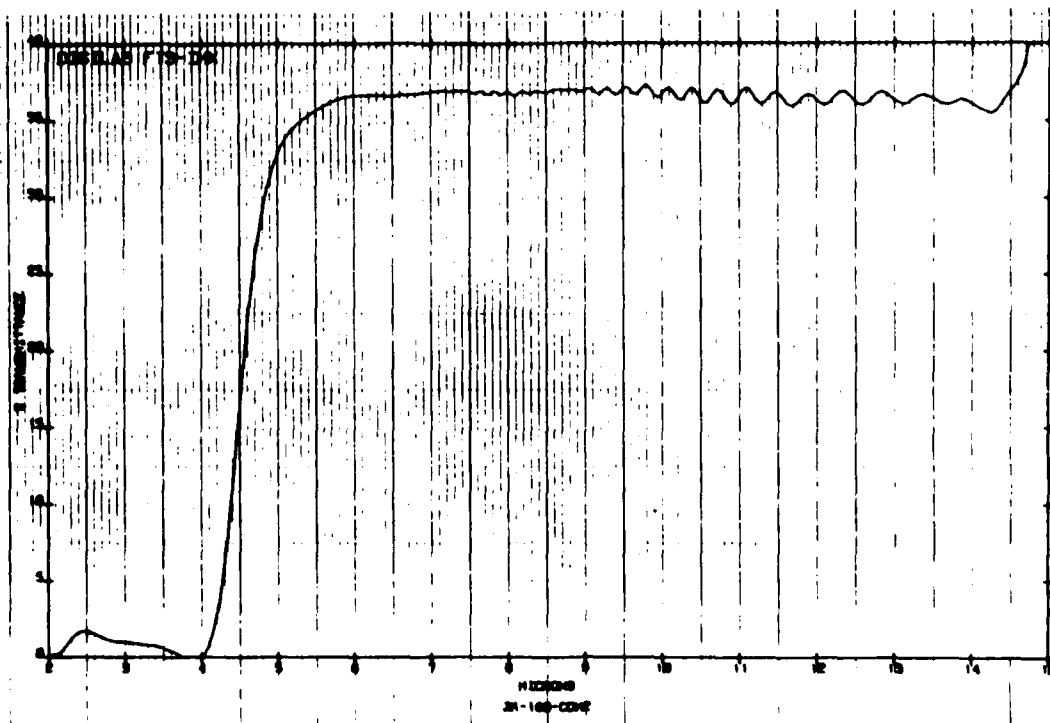
Figure 51 from Final Report. This is the uncalibrated
FTIR spectra of HgCdTe epitaxy part Cd160.

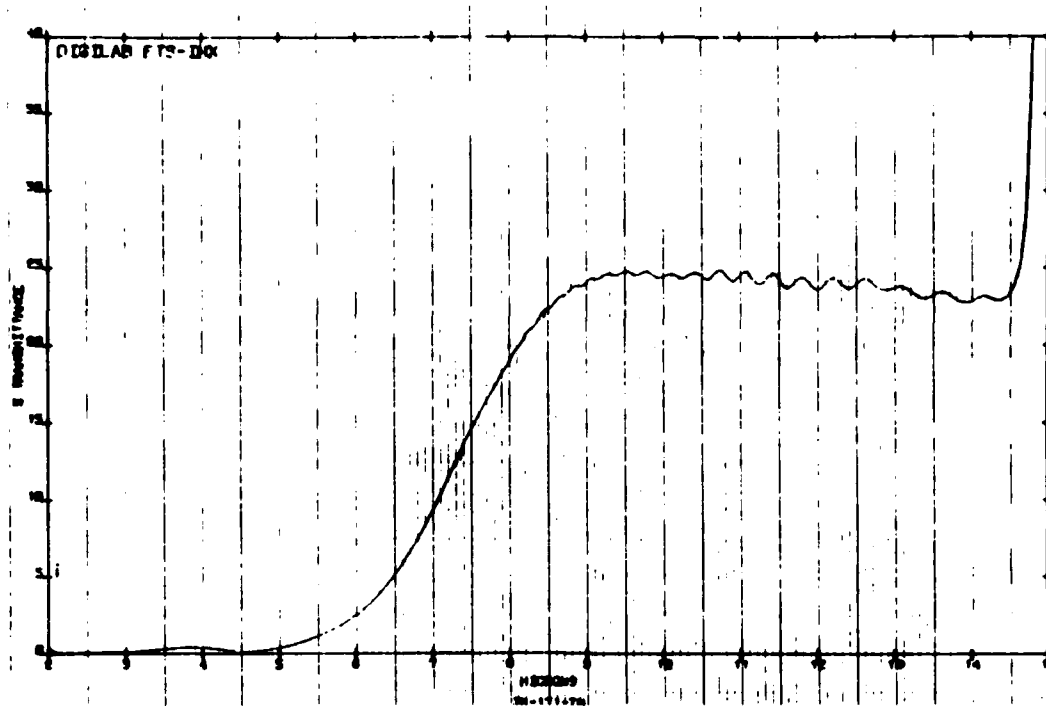Figure 51, part Cd160, after the FTIR calibration.

Figure 55 from Final Report. This is the uncalibrated
FTIR spectra of HgZnTe epitaxy part Zn171, indicating
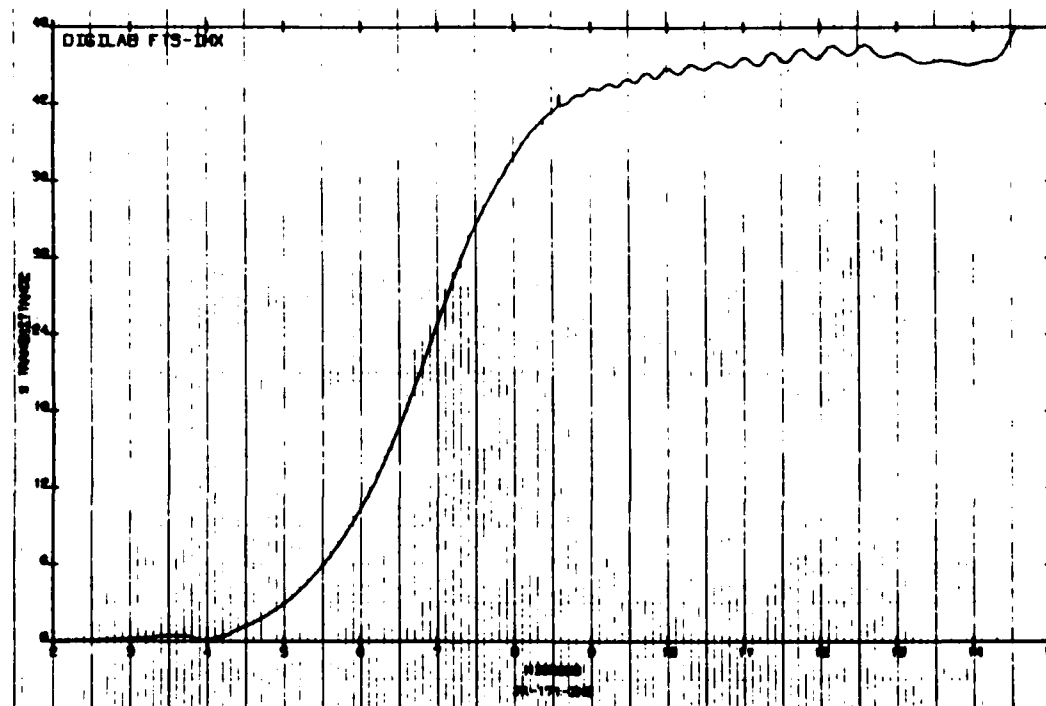a cutoff wavelength of 7.3 microns.

Figure 55, after calibration, showing a 6.8 cutoff and
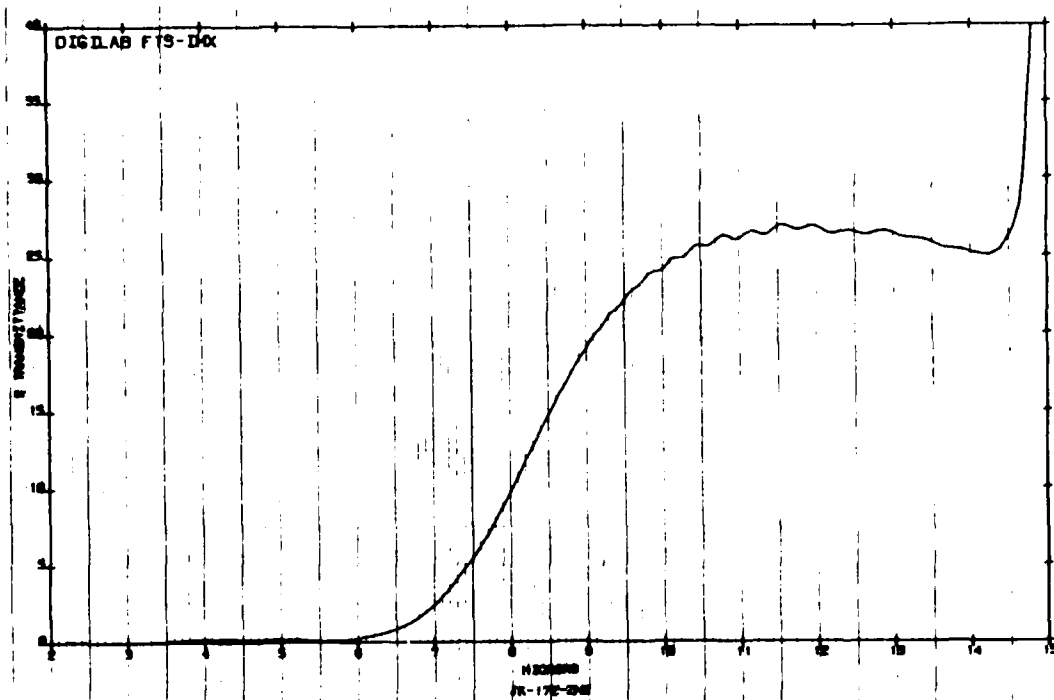a 75% increase in transmittance (from 25% to 44%).

Figure 56, calibrated FTIR of part Znl72, indicating
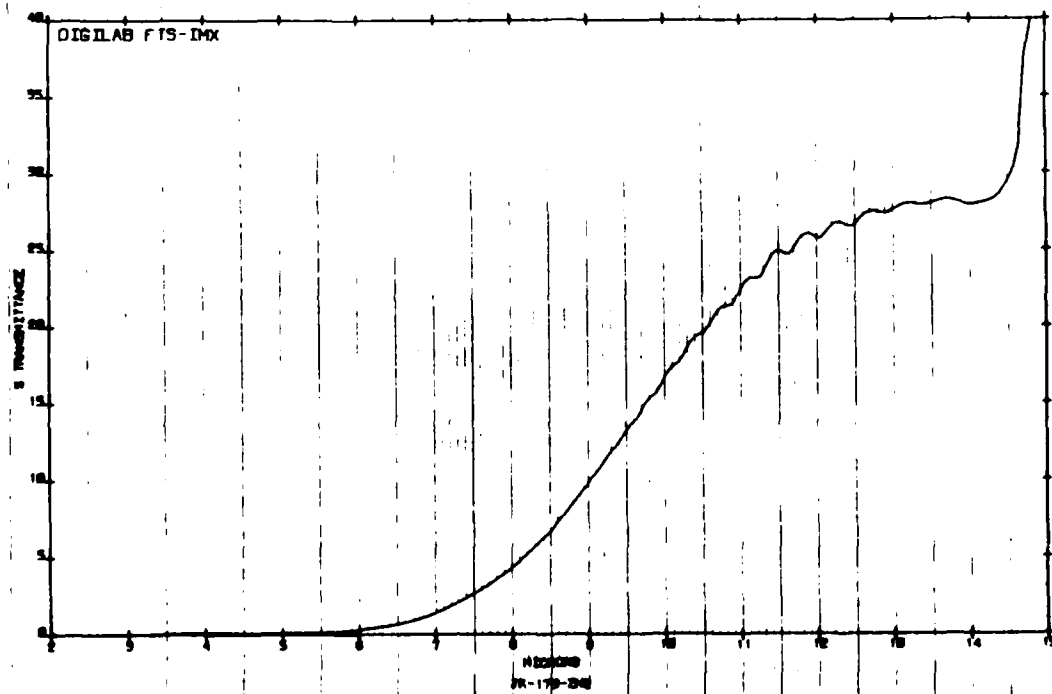a cutoff wavelength of 8.5 microns.

Figure 57, calibrated FTIR of part Znl73, indicating
a cutoff wavelength of 9.7 microns.

END
DATE
FILMED
7-88
DTIC